Addressing the Mars ISRU Challenge:
Production of Oxygen and Fuel from CO$_2$ Using Sunlight

Keck
INSTITUTE FOR SPACE STUDIES

Addressing the Mars ISRU Challenge:

Production of Oxygen and Fuel from CO$_2$ Using Sunlight

Study Co-leads: Will West (JPL), Harry Atwater (Caltech), Cliff Kubiak (University of California, San Diego)

Study Participants: Xenia Amashukeli (Caltech), Shane Ardo (University of California, Irvine), Manan Arya (JPL), Christopher Bates (Caltech), Erik Brandon (JPL), Wen-Hui (Sophia) Cheng (Caltech), John Graf (NASA Johnson Space Cener), Jonathan Grandidier (JPL), Jeffery Greenblatt (Lawrence Berkeley National Laboratory), Joel Haber (Caltech), Michael Hecht (Massachusetts Institute of Technology), Stephen Hoffman (Science Applications International Corporation), John Hogan (NASA Arms Research Center), Frances Houle (Lawrence Berkeley National Laboratory), Simon Jones (JPL), David Kass (JPL), Matt Law (University of California Irvine), Amir Mazaheripour (University of California, Irvine), Brendon McNicholas (Caltech), Anne Meier (NASA Kennedy Space Center), Adam Nielander (Caltech), Bruce Parkinson (University of Wyoming), Arvind Ramachandran (Arizona State University), Gerald Sanders (NASA Johnson Space Center), Samuel Schreiner (JPL), Valerie Scott (JPL), Ellen Stechel (Arizona State University), Karl Walczak, Lawrence Berkeley National Laboratory), Adam Weber (Lawrence Berkeley National Laboratory), Chengxiang ("CX") Xiang (Caltech), Jenny Yang (University of California, Irvine), Almagul Zhanaidarova (University of California, San Diego)

Contents

List of Figures

Executive Summary

Advanced exploration of Mars, particularly human missions, will require vast amounts of fuel and oxygen for extended campaigns and the return of samples or humans back to Earth. If fuel and oxygen can be prepared on Mars from in-situ resources, this would greatly reduce the launch mass of the mission from Earth. In this Keck Institute for Space Sciences (KISS) study, the viability of Mars near-ambient temperature photoelectrochemical (PEC) or electrochemical (EC) production of fuel and oxygen from atmospheric carbon dioxide—with or without available water—was examined.

With PEC devices incorporated into lightweight, large-area structures operating near 25°C and collecting solar energy to directly convert carbon dioxide into oxygen, it may be possible to reduce the launch mass (compared with bringing oxygen directly from Earth) by a factor of three or more. There are other numerous benefits of such a system relative to other in-situ resource utilization (ISRU) schemes, notably reduced thermal management (e.g., lower heating demand and decreased amplitude of thermal cycling) and the elimination of a need for a fission power source.

However, there are considerable technical hurdles that must be surmounted before a PEC or EC ISRU system could be competitive with other more mature ISRU approaches, such as solid oxide electrolysis (SOXE) technology. Noteworthy challenges include: the identification of highly stable homogeneous or heterogeneous catalysts for oxygen evolution and carbon monoxide or methane evolution; quantification of long-term operation under the harsh Martian conditions; and appropriate coupled catalyst–light absorber systems that can be reliably stowed then deployed over large areas, among other challenges described herein.

This report includes recommendations for future work to assess the viability of and advance the state-of-the-art for EC and PEC technologies for future ISRU applications. Importantly, the challenges of mining, transporting, purifying, and delivering water from Mars resources to a PEC or EC reactor system, development and demonstration of a low-temperature-capable, non-aqueous-based CO_2 reduction scheme as described below is perhaps the first logical step toward implementing an efficient near-surface Mars temperature oxygen generation system on Mars.

1. Overview of Workshop Goals

An ongoing challenge in the long-term campaign to explore Mars is the mass and complexity involved in transporting consumables from Earth to the Martian surface. Key mission consumables are oxygen and fuel, which are planned to be used for crewed ascent from the Mars surface. These consumables are also critical for providing a breathable atmosphere, as a reactant for power generation from fuel cells, and for the production of other consumables necessary for human missions on Mars.

Previous studies have shown that in-situ resource utilization (ISRU) provides a viable pathway for supplying fuel and oxygen to these mission applications by reducing readily available carbon dioxide from the Martian atmosphere for oxygen and producing fuel with either locally-obtained water or hydrogen brought from Earth. Ambient carbon dioxide reduction is likely to minimize or even eliminate the need to transport large quantities of oxygen from Earth to Mars. To successfully support crewed ascent from the Mars surface, large amounts of fuel and oxygen (e.g., 15 to 20 metric tons per Martian year) will be needed, necessitating development of approaches to carbon dioxide reduction.

This Keck Institute for Space Sciences (KISS) study examined the viability of the photoelectrochemical (PEC) or electrochemical (EC) production of fuel (e.g., carbon monoxide or methane) and oxygen from atmospheric carbon dioxide and, if available, mined and purified water on Mars. Rather than using a high-temperature solid oxide electrolysis process, sunlight would either be used directly with a catalytic process to effect the low temperature conversion of carbon dioxide to fuel and oxygen using large-area deployable PEC panels, or photovoltaic-powered electrochemical conversion would be employed at near-Mars surface ambient temperatures.

The workshops held in July and August of 2016 brought together experts in this field to develop a path forward for solving the Mars ISRU challenge of using sunlight for mission consumable production. The main technical goals were to identify specific low-temperature, low-mass, low-energy pathways that are well suited for carbon dioxide reduction in the unique Mars environment, as well as viable designs for scalable Mars oxygen and fuel production systems.

2. Basis of Comparison

There are several approaches for converting Mars atmospheric CO_2 (and, if available, H_2 and H_2O) into useful products, including oxygen (O_2) and methane (CH_4). One method for converting CO_2 to O_2 is through solid oxide electrolysis (SOXE), a concept that dates back to the early 1980s (*Richter*, 1981; *Frisbee et al.*, 1987; *Crow*, 1997). SOXE utilizes a ceramic oxide conductor to which an electric current is applied. At high temperatures (800-1000°C) and at the surface of a catalyst, oxygen is removed from the CO_2 and transferred through the ceramic oxide membrane to the other side, leaving behind carbon monoxide (CO) and unreacted CO_2. Another process under consideration to make only oxygen is the Reverse Water Gas Shift process where CO_2 is combined with hydrogen (H_2) at elevated temperatures (>450°C) and pressures to make CO and water (H_2O). The water is then split into oxygen and hydrogen; the O_2 is stored and the H_2 is recycled. If methane fuel is also desired, the currently preferred approach is to utilize the Sabatier process, which combines CO_2 and H_2 to form CH_4 and H_2O. Since more H_2 is needed to make methane than is recycled from the H_2O produced, extra hydrogen or water from Earth or in-situ resources is required. The attractiveness of the SOXE process lies in the fact that it does not require other chemical feedstocks (such as H_2) to support the conversion of CO_2 to a useful product, and it is a solid state device that produces pure, dry oxygen.

A demonstration of the SOXE technology is planned as part of the Mars 2020 rover, the Mars Oxygen ISRU Experiment (MOXIE; *Sridhar et al.*, 1997; *Hecht et al.*, 2015; *Hartvigsen et al.*, 2015; *Meyen et al.*, 2015; *Rapp*, 2016), which builds on earlier demonstrations such as the Mars Oxygen Cells (MOXCE) project (*Crow*, 1997). The goal of the flight experiment is to demonstrate a sub-scale O_2 generation plant on Mars under actual Mars environmental and atmospheric conditions over an extended period of time.

In looking toward the future, there are various roadmaps and architectures that feature the use of O_2 production on Mars (*Rapp*, 2016; *Drake et al.*, 2009; *Rucker et al.*, 2016; *Sanders et al.*, 2015). One of the key uses is to support a Mars Ascent Vehicle (MAV) propellant system. Since approximately 78% of the reactant mass is O_2 for a O_2/CH_4 based chemical propulsion system, this would provide a significant benefit to any mission with respect to launch mass. Preliminary mission models suggest that up to 30,000 kg of oxygen will be required as the oxidant for this ascent vehicle, which would require 2 to 3 heavy lift launches if brought directly from Earth to Mars (*Richter*, 1981). Current approaches target the production of 25–30 metric tons of oxygen over a 14 to 17 month time frame at a rate of 2–3 kg/hour (*Rapp*, 2016; *Drake et al.*, 2009; *Rucker et al.*, 2016; *Sanders et al.*, 2015). It should be noted here that CO as an ascent vehicle fuel is impractical relative to the high energy content of CH_4, though as a byproduct of an EC or PEC reduction of CO_2, CO may serve as a lower-energy-content fuel for other energy conversion applications on Mars.

A concern regarding SOXE-based approaches is the significant power required to support the electrolysis current, as well as to provide make-up heating to maintain sufficient stack temperatures. According to the latest calculations, the MOXIE demonstration payload is projected to require up to 300 W of power to support what is anticipated to be about a 0.45% demonstration (i.e., ~10g O_2/hr); this suggests that the power required to scale up to requisite production levels is on the order of ~66 kW, although this likely overestimates the power level due to non-linear scaling of heat leakage, electronics and other system factors (*Hecht et al.*, 2015). A detailed system design would be required to establish a high fidelity value. Other analyses suggest that baseline SOXE designs will require 30–45 kW of power for a 3 kg/14 month (420 sol) scenario, with approximately 20 kW required for the SOXE unit alone (*Rapp*, 2016). Design Reference Architecture-5 (DRA-5) notes power levels on the order of 26 kW (operating continuously) when using a fission power source (FPS) and 96 kW (operating eight hours/day) for a solar array approach (*Drake et al.*, 2009). A summary of the mass and power levels from these various studies is noted in Table 2.1.

Source	O_2 Production Rate (kg/h)	Power (kW)	SOXE Plant Mass (kg)	Solar Array Mass (kg)	FPS Mass (kg)	Total Mass (PV+plant) (kg)
DRA-5[a]	2.2	26 (FPS) 96 (SA)	900	14,595	7,800	15,495
COMPASS[b]	2.2	26	671	17,815	9,154	18,486

Table 2.1: Estimated Mass and Power Required for SOXE-Based ISRU Architectures.

[a] *Drake et al.* (2009)
[b] *Sanders et al.* (2015)

Taking a value of 25 kW as a starting point, there are two options to supply these levels of power: solar arrays and FPS. To date, the United States has flown one fission reactor in space

(1965). Since then, NASA has made several attempts to design and fly a nuclear power reactor. In recent years, NASA has funded the Kilopower project to develop a low temperature nuclear power reactor (*Gibson et al.*, 2017). However, given the low TRL with respect to an FPS and the political issues associated with testing and launching nuclear reactors, the solar array approach is further evaluated here. A solar array module (which includes the photovoltaics, support structure, and electronics) to produce 5 kW of power has been estimated to have a mass of 2,919 kg per module, or 14,595 kg total for 25 kW capability (*Hecht et al.*, 2015). A 30-kW fission power system has also been proposed at 7,800 kg per unit (*Hecht et al.*, 2015).

A recent study from a NASA COMPASS team indicated a 1/5-scale ISRU plant would be 192 kg and a full production model would be 671 kg (*Sanders et al.*, 2015). The total mass of a SOXE-based system includes the chemical plant plus the power generation scheme required to operate it. To be viable, this total mass must be lower than the total mass of O_2 required (30,000 kg). The total mass of the system above is 18,486 kg. This provides a mass leverage (the ratio of the mass of carried oxygen to the mass of an in-situ oxygen production plant) of about 1.6. An FPS could be deployed to improve this advantage, but this requires parallel development of two low TRL technologies: a full scale SOXE plant and an FPS. Furthermore, given the generally unfavorable public perception of using fission reactors for spacecraft applications, this presents an unknown risk for long-term support for FPS development.

Table 2.2 below provides an analysis of a representative SOXE-based plant, along with the mass and power fraction that each subsystem contributes to the total system. From this, the potential advantage of a PEC system can be considered by recognizing that certain sub-systems will be common to both (i.e., filtration, storage, etc.). As seen below, scale-up to full production will require ~20 kW for the SOXE stack, in line with what is reported in *Rapp* (2016) for a similar scale of production, with ~35 kW total required at scale.

If the basic chemical processing plant for a full-sized unit is 671 kg and a maximum of 18% of the mass could be saved by using PEC technology, this represents 120 kg of mass saving. Most significantly, if 20,433 kg of solar array modules is required to run the full SOXE system (35 kW) and the power to operate just the chemical plant could be reduced by a maximum of 39% by switching to a PEC device, then up to 8,757 kg could be saved from power considerations alone (only 20 kW solar array required). If the total mass contribution of the SOXE plant and the power systems required to run it could be reduced by 8,877 kg (as above), the total system mass could be brought to 11,566 kg, thus increasing the mass leverage to almost 3. This is a significant benefit to future Mars architectures. With lightweight, large-area PEC structures, it may be possible to reduce the mass even further. In addition, thermal considerations are much less significant with PEC systems as the temperature swings experienced by the device on a diurnal basis are much less than for SOXE (i.e., ambient to ~25°C vs. ambient to 800°C) and material thermal expansion coefficient mismatches are less important; hence, device reliability may be improved as a result. Note also that the SOXE mass estimates from the MOXIE demo

Subsystem	Mass (kg)	Mass Fraction (%)	PEC Approach	Max Mass Savings (%)	Power (kW)	Power Fraction (%)	PEC Approach	Max Power Savings (%)
Filtration	1.23	0.4	Common		0.00025		Common	
CO_2 Collection/ Freeze	173	53	Common		2.23	33	Common	36
SOE Processor	5.6	1.7	Use PEC Device	1	3.7	55	Use PEC Device	
SOE Recirculation System	34.6	11	Use PEC Device	8	0.187	3	Use PEC Device	3
SOE Device Housing	42.7	13	Lightweight materials (reduced thermal tolerance required)	9				
O_2 Liquefaction and Storage	70	21	Common		0.6	10	Common	
Total	**327**	**100**		**18%**	**6.72**	**100**		**39%**

Table 2.2: Breakdown of 0.45 kg/hr or 1/5 demonstration SOXE plant (*Sanders et al.*, 2015).

continue to increase as the project develops toward a flight demonstration (increasing from 168 W for a 1% demo from initial projections to 300 W for a 0.45% demo at the time this report is going to press.[1]).

This report will focus on exploring several options that address the above challenge. In one option, the approach includes using photovoltaic-powered EC versus direct PEC conversion of the reactants. In the PEC case, two options are discussed: one in which the only feedstock is CO_2—referred to as non-aqueous PEC—and the other including a provision to produce CH_4 for propellant, leveraging planned resources to harvest water from the Mars regolith and further increase the benefits of such a system. In the case that water is available, the aqueous PEC systems assume the availability of purified water from the Martian surface. The non-aqueous PEC systems produce oxygen and CO without using water as a consumable, but may use water as a solvent for the reactions. The former system is considered first.

We note that, for the discussions below, we consider any system in which the energy input is from solar sources to be a "PEC" system. Of course, there are many variants for system-level implementation that can be envisaged, such as

(i) Landed photovoltaic power source (e.g., solar array) connected to an electrolysis reactor (with or without battery or similar energy storage device),

---

[1]https://mars.nasa.gov/mars2020/mission/instruments/moxie/, accessed October 2017

(ii) Direct photo-driven electrolysis reactor, without energy storage or alternative power source,

(iii) Orbiting photovoltaic power source supplying power to landed electrolysis reactor via power beaming.

Initially, we will study fundamental electrolytic processes that we consider to be the most promising for implementation on Mars at lower temperatures than those required by SOXE or other processes (e.g., Sabatier). We highlight the pressing need for characterization of these reactions under Mars-relevant conditions (temperature and pressure) so that a direct comparison with SOXE implementations can be performed at the system level to guide future mission architecture planning. In addition, we note that direct electrolysis reactors can receive power input from any electrical source, and are thus compatible with radioisotope thermoelectric generator (RTG) or fission power system architectures without requiring substantial modification.

3. Aqueous PEC System

Of the many approaches to the design of aqueous CO_2 reduction devices for application on Mars, two device configurations are considered here. The first configuration, Device-A, is essentially an oxygen generator, where the anode reaction is $H_2O + 2\,h^+ \longrightarrow \frac{1}{2}O_2 + 2\,H^+$, and the cathode reaction is $CO_2 + 2\,H^+ + 2\,e^- \longrightarrow CO + H_2O$. Note that there is no net water consumption in the overall reaction; the water is simply transported from the anode chamber into the cathode chamber during the reaction. Hence, a recirculation of water will be necessary in the Device-A configuration to ensure zero net water consumption during the process. As a result, Device-A does not rely on the water resources on Mars and does not provide the fuel needed for the ascent vehicle. Device-A is relatively low risk with key materials available today. Device-A will also be able to provide direct comparison to the MOXIE system.

Device-A will consist of a power-generating component, a fuel-forming component, and auxiliary systems. The power-generating component could consist of ultra-light-weight PV modules, in which state-of-the-art cells with a solar-to-electric conversion efficiency of 30% and a specific power density of 2kW kg^{-1} can be used. The fuel-forming component will consist of CO_2 reduction catalyst, oxygen evolution catalyst, electrolyte media, and membrane separators. Various CO_2 reduction catalysts, including oxide-derived Au (*Chen & Kanan*, 2012), nanoporous Ag (*Lu et al.*, 2014), metal chalcogenide (*Asadi et al.*, 2016), etc., exhibited active and selective electrocatalytic properties for CO_2 reduction to CO. For instance, recent reports on nanostructured transition metal dichalcogenide electrocatalysts showed that an operating current density exceeding 50 mA cm^{-2} can be obtained at <100 mV overpotential for selective CO_2 reduction to CO (*Asadi et al.*, 2016). As for the electrocatalysts for oxygen evolution reaction (OER), metal oxides and mixed metal oxides, including NiO_x (*Sun et al.*, 2015), $NiFeO_x$ (*Batchellor & Boettcher*, 2015), $NiFeCoCeO_x$ (*Haber et al.*, 2014) in alkaline conditions (*Jung et al.*, 2016) and IrO_x or

mixed IrO_x in acidic conditions (*McCrory et al.*, 2015), showed stable and active performance with a typical overpotential of 250 mV at the operating current densities that match the solar photon flux. A range of electrolyte media can be employed in such a device, including an aqueous bicarbonate buffer solution or ionic liquids. The separation between the cathode and anode chambers, as well as the ionic transport between the two chambers, is often realized by the use of polymer membranes. Depending on the selection of catalyst materials, proton conductive membranes, such as Nafion, or hydroxide conductive membranes, such as Selemion, or a mix of cation and anion exchange membranes, such as bipolar membranes, will be used. The power-generating component and the fuel-forming component will be fully integrated together and the geometric operating current density of ~5 mA cm^{-2} would be the target generation rate for the system. The auxiliary systems in Device-A will include the transport and delivery of 1 atm CO_2 and water to the catalytic sites, recirculation of the water generated at the anode to the cathode, and efficient collection and separation of O_2 from CO. For Device-A, a total cell voltage, which includes the thermodynamic voltage for the CO_2 reduction and oxygen evolution reaction, kinetic overpotentials for the two reactions, concentration overpotentials at the electrode surfaces, and transport losses in the electrolyte and membrane, is expected to be ~2 V. Based on the performance of the state-of-the-art CO_2 reduction catalyst, a Faradic efficiency of 90% is expected. Hence, the overall solar-to-fuel conversion efficiency for Device-A is expected to be ~15–18% with a 30% efficient PV module.

Device-B is an aqueous-based methane generator, in which methane will be generated at the cathode surface, oxygen will be generated at the anode surface, and water will be consumed in the process to provide protons resulting in fuel generation. The major components and system architectures in Device-B are very similar to Device-A. The only difference is the required electrocatalysts for CO_2 reduction to methane at the cathode. Currently, there are few electrocatalysts reported to perform CO_2 reduction to methane at high activity and selectively. Moreover, the mechanism for this eight-electron, eight-proton reaction is still under debate. Copper or copper-derived catalysts are among of the most studied materials systems that exhibit moderate selectivity towards methane. For instance, a Faradic efficiency of 33.3% at >1.0 V of overpotential was reported by *Hori et al.* (1989) and similar performances in copper based systems have been observed in recent years as well. More recently, rhodium nanomaterials have been described with promising potential for this process (*Zhang et al.*, 2017). Based on the performance of Cu as the electrocatalyst for methane, a cell voltage of ~3.4–3.5 V is expected with a Faradic efficiency of ~30%. Hence, Device-B with the state-of-the-art materials assemblies is expected to deliver an electric-to-fuel conversion efficiency of ~10–15% and an overall solar-to-fuel conversion efficiency ~3%–4.5%.

Because of the different technology readiness levels for Device-A and Device-B, different emphases in research development could be taken for the two systems. For Device-A, since existing materials could already deliver >10% efficient systems, full cell prototyping under realistic operating

conditions is critical to advance this concept. Moreover, development of the membrane-electrode assembly, engineering of the reactant/product delivery and transport, and optimization of the prototype geometries are also needed to demonstrate an efficient, stable prototype. In-depth architecture modeling using multi-physics computational simulations will also provide vital design guidelines and reveal the most effective levers in the system for the Mars ISRU application. Moreover, it would be very valuable to provide quantitative analysis based on experimental results that compare Device-A with MOXIE under operation to understand the pros and cons of the two systems. In contrast, the development of Device-B should focus on catalyst and reaction engineering and understanding the underlying mechanism for the coupled multi-electron, multi-proton reaction. Development of more efficient and selective electrocatalysts for CO_2 reduction to methane is a prerequisite for an efficient system. It would also be very valuable to perform quantitative analysis that compares Device-B with a step-wise approach that couples a water electrolysis reactor and a Sabatier reactor.
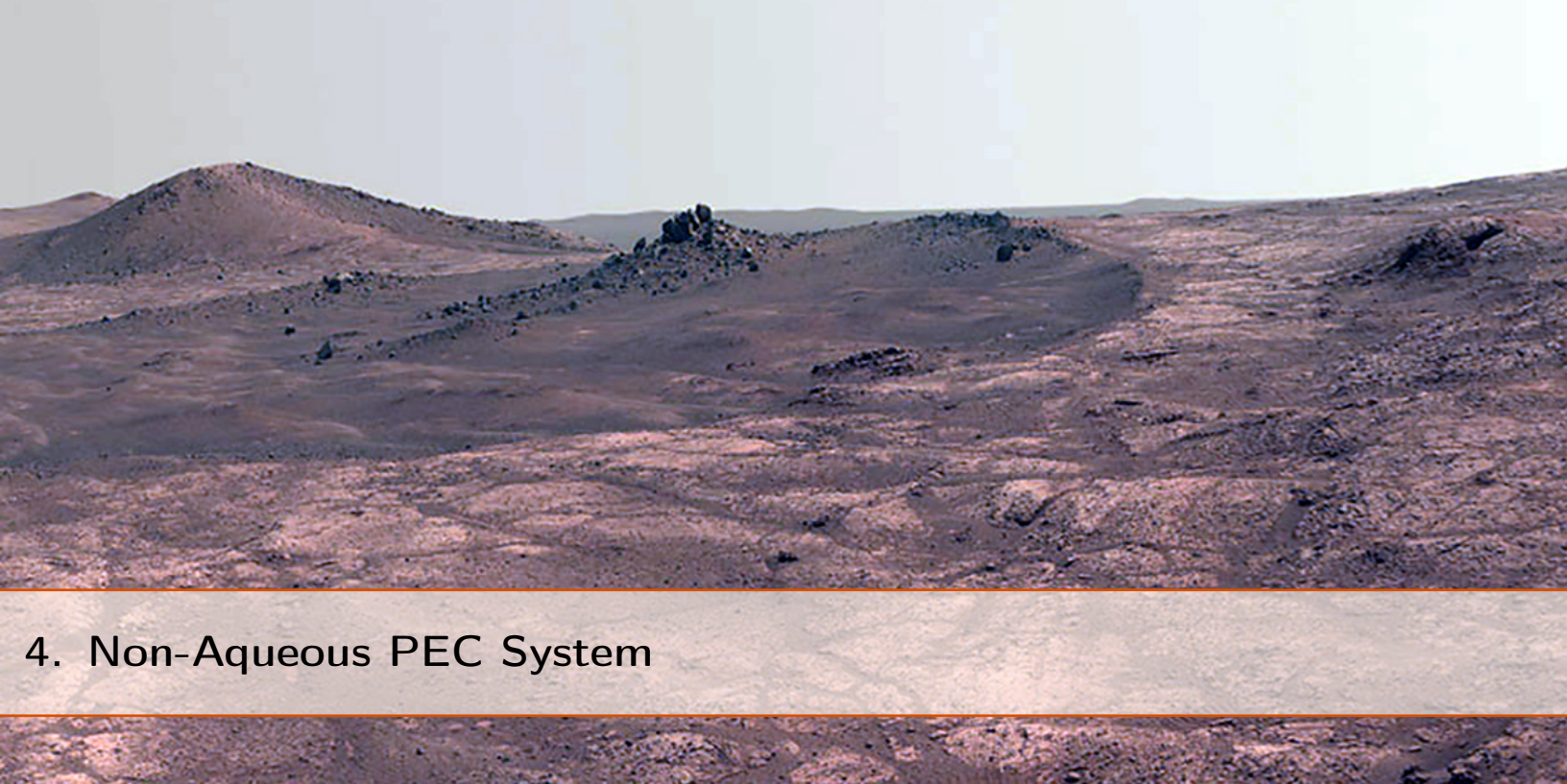
4. Non-Aqueous PEC System

4.1 Introduction

Due to the difficulty, complexity, and mission risk associated with extracting water from resources on Mars, achieving electrochemical splitting of Martian atmospheric CO_2 through a non-aqueous process represents an interesting alternative ISRU strategy for generating O_2 (for life support and propellant oxidizer) and low-grade fuel (CO) in situations when maintaining and recycling water is challenging. Systems based around this concept might necessarily be more flexible operationally than aqueous approaches, so they could be able to be deployed to multiple sites across the Martian landscape and/or carried on-board an EVA Rover supporting extended missions away from a central base. These systems can also be designed to be lightweight and self-sufficient, requiring no other inputs than sunlight and atmospheric CO_2 to function. Eventually, such systems could be landed at various points across Mars and may act as "refueling stations" for Rovers or Hoppers, emergency life-support stations, and/or propellant sources for Mars Sample Return missions (with both O_2 and CO being available). They are also potentially scalable in similar fashion to aqueous PEC designs, so that they can be installed directly at the landing site as an alternative source for the large volumes of O_2 required for MAV propellant applications. However, the fundamental electrochemistry and materials set useful for these systems is at a much lower technology readiness level (TRL) than for aqueous approaches, so the focus of the majority of the discussion in this section aims to explore the various possibilities that have been identified from prior work in the literature, and to call out interesting targets for R&D opportunities to help accelerate the maturation of this concept toward a working demonstration useful for Mars ISRU missions in a relatively short timeframe ("Device-C").

It is believed that the majority of the system-level considerations (e.g., power input, O_2 generation requirements, sub-systems such as atmospheric processing, thermal management, gas storage, and concept of operations) are similar to those described in detail in the aqueous PEC section for Device-A and Device-B and/or at a much lower resolution for their requirements due to the fundamentally-lower TRL of the non-aqueous technology. Hence, this section of the report will not spend much time discussing system-level requirements but will instead focus on concepts and immediate needs.

A general overview of a suitable non-aqueous electrochemical concept is shown below in Figure 4.1, with a detailed discussion in the following section:
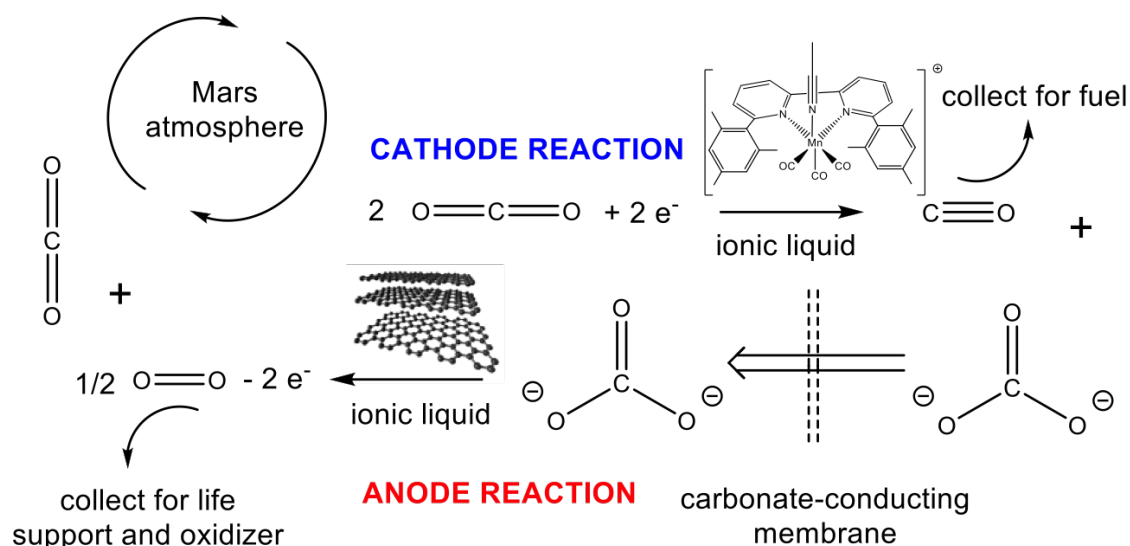
Figure 4.1: General concept for non-aqueous electrochemical CO_2 splitting on Mars using CO_3^{2-} as the carrier ion.

The cathode reaction involves the dimerization and disproportionation of CO_2 in the presence of a suitable catalyst to give CO and carbonate anion (CO_3^{2-}); the CO is collected and stored, for potential use as fuel, while CO_3^{2-} is transported across a membrane where it releases O_2 upon oxidation at the anode, regenerating CO_2, which is fed back into the system. Thus, this electrochemical cycle operates in the absence of water, utilizing CO_3^{2-} as the carrier species. Several elements of this cycle (i.e., the CO_2 reduction half-reaction) have been shown to work quite well on Earth under relatively benign conditions (i.e., 1 bar CO_2 pressure, 25°C) but have not been investigated under conditions more relevant to Mars (lower total and CO_2 pressure and lower temperatures), so establishing the envelope of their useful operation in this context is an immediate R&D requirement. In other cases, no suitable material to enable a full cell demonstration is known, so exploratory materials R&D work is necessary.

4.2 Fundamental Electrochemistry and Materials Technology

4.2.1 Cathode Reaction: CO_2 Reduction via Dimerization/Disproportionation

4.2.1.1 Homogeneous Catalysis: Mn(mesbpy)

Earlier reports from the Kubiak group (cf. *Ratiff et al.*, 1986–1988; *Lewis*, 1993) describe a solid-state p-GaP semiconductor PEC device with Ni_3-cluster electrocatalyst for the CO_2 splitting to CO and O_2. A prototype electrochemical device for the CO_2 splitting would consist of a cathode chamber with a molecular CO_2 reduction catalyst, an anode chamber for oxygen production, and an ion selective membrane in between. The catalyst will selectively disproportionate CO_2 to CO and carbonate (CO_3^{2-}), of which the CO_3^{2-} will pass through the membrane and be oxidized at the anode to provide O_2. Thus both CO and oxygen will be produced by this device.
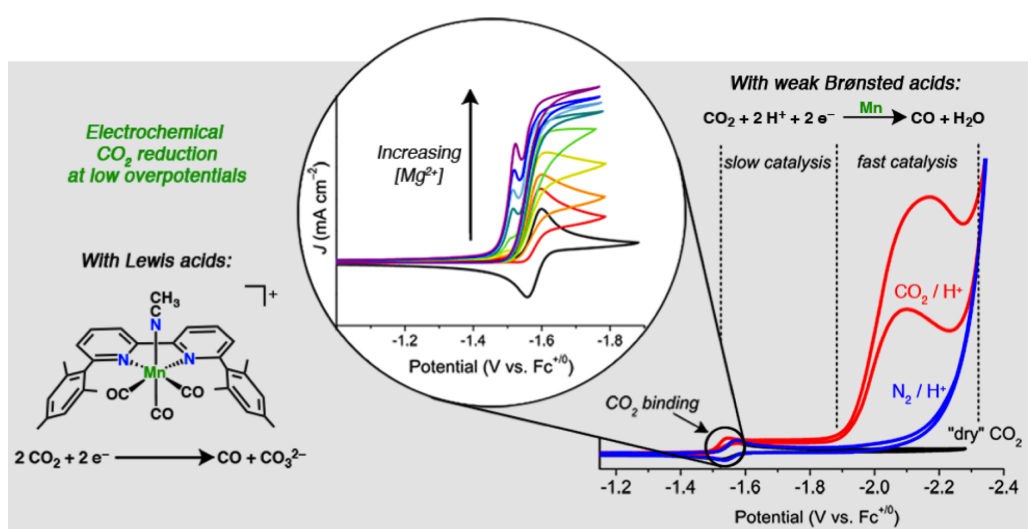
Figure 4.2: Electrochemical CO_2 reduction by Mn(mesbpy) catalyst with Lewis acids and with weak Brønsted acids (Adapted with permission from *Sampson & Kubiak*, 2016).

A recent investigation of the catalyst Mn(mesbpy)(CO)$_3$Cl and its catalytic reactivity with Lewis acids (*Sampson & Kubiak*, 2016) provides a recent illustration of the operating principles necessary for the development of a molecular catalyst for non-aqueous CO_2 reduction to CO and carbonate. Here, conversion of CO_2 to CO and carbonate occurs in the presence of a Lewis acid Mg(OTf)$_2$ at room temperature with the lowest overpotential (η) ever reported for molecular CO_2 reduction electrocatalysts ($\eta = 0.30$–0.45 V). Formation of CO and carbonate proceeds via the desired reductive disproportionation of CO_2 ($2\,CO_2 + 2\,e^- \longrightarrow CO$ and CO_3^{2-}). This catalyst operates in dry acetonitrile at -1.60 V vs. $Fc^{+/0}$ with a Faradaic efficiency of $98 \pm 2\%$ and a turnover number (TON) of 36 after 6 hours of electrolysis. The formation of CO, CO_3^{2-} and HCO_3^{2-} was

confirmed with gas chromatography, FTIR, and infrared-spectroelectrochemistry (IR-SEC) during and after the experiment.

Accumulation of the insoluble carbonate salt is the main problem for the described system. This issue can be overcome by utilizing a sacrificial Mg-anode to prevent precipitation (by creating soluble Mg carbonate salts) and to increase the catalytic turnover. However, such an approach is clearly not sustainable, and other solutions such as the use of soluble Lewis acids need to be identified. A broad variety of Lewis acids should be tested for use together with the Mn(mesbpy) catalyst to prevent formation of carbonate precipitates.

Other CO_2 reduction catalysts like Re(pby)(CO)$_3$ (*Hawecker et al.*, 1984) and Ni(cyclam) (*Froehlich & Kubiak*, 2015), are well known for their ability to reduce CO_2 to CO in the presence of a proton source (H$_2$O, TFE, PhOH) through a proton-coupled electron transfer mechanism. These molecular catalysts could also be used as potential candidates for CO and carbonate production under anhydrous conditions.

4.2.1.2   Heterogeneous Catalysis: CO_2 Reduction by Lead

Heterogeneous CO_2 reduction in aqueous solutions on metal electrodes is thoroughly described by *Hori* (2008). Unfortunately, the majority of these electrodes (e.g., Cu) tend to have low selectivity towards CO and produce a mixture of products. Lead and mercury electrodes, however, can reduce CO_2 to CO and an equimolar amount of carbonate. According to *Gennaro et al.* (1996), mixtures of CO and oxalate were formed during the direct electrolysis of CO_2 at –2.21 V vs. SCE in DMF using a mercury electrode. It was shown that the yield of CO and carbonate depended on the concentration of CO_2 in the reaction mixture as well as the operating temperature. The yield of CO decreased with the decreasing concentration of CO_2, while steady increase of the CO yield was observed with the decreasing temperature (25°C to –20°C). Similar results were found using a lead electrode, which would be the more ideal device candidate.

Coupling of two radical ions $CO_2^{\bullet-}$ under electrochemical reduction conditions resulted in the formation of oxalate. CO and carbonate formed during the electron transfer reaction between CO_2 and $CO_2^{\bullet-}$.

4.2.2   Anode Reaction: O_2 Oxidation

Electrochemical water oxidation on precious metals and metal oxide semiconductor surfaces (e.g., TiO$_2$, NiO$_x$, FeO$_x$, IrO$_x$, WO$_3$) is a widely studied process and can be used as a platform for carbonate oxidation to diatomic oxygen. We note that the concept for the non-aqueous process was originally described by described by the Kubiak group (cf. *Ratiff et al.*, 1986–1988; *Lewis*, 1993) as shown in Figure 4.4 (*Breedlove et al.*, 2001). Although the Ni$_3$ cluster catalyst shown is sub-optimal for the CO_2 reduction process (being superseded now by the Mn-Mg species described
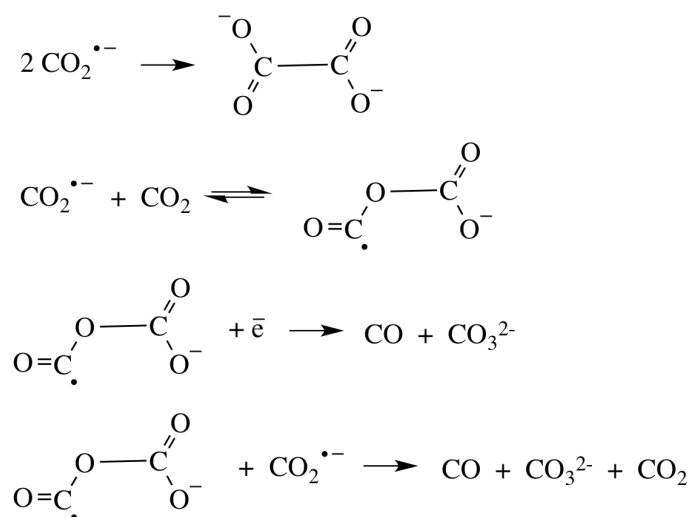
Figure 4.3: CO_2 reduction mechanism on a lead electrode. Adapted from *Gennaro et al.* (1996).

above), the oxidation of carbonate species by the photogenerated holes (h^+) that occurs on the dark side of the device represents an interesting potential method for oxygen formation in a full cell based on this concept. However, it is likely that a greater efficiency will be derived from a coupled PV-electrolyzer system than a direct photo-absorbing PEC system, so system-level considerations will most likely point to development of alternative anodes.

Carbonate oxidation to give O_2 may be considered to be the reverse of the cathode process occurring in a carbonate fuel cell:

$$\tfrac{1}{2}\,O_2 + CO_2 + 2\,e^- \longrightarrow CO_3^{2-}$$
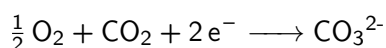
These fuel cells operate at high efficiencies (~60%) using a molten carbonate salt (Na and K carbonates) at temperatures above 600°C. This high temperature requirement is mainly imposed by the melting point of the electrolyte salts; the requirement for molten salts comes from the dominance of side-reactions (e.g., water splitting) if aqueous solutions are employed instead. Hence, it is reasonable to project that a low-temperature variant could be designed whereby efficient CO_3^{2-} oxidation to O_2 may be achieved if a suitable solvent is found that is capable of dissolving substantial quantities of carbonate salt while remaining stable at the operating potential of the oxidation process. Solutions of alkali metal carbonates (e.g., Li_2CO_3) in ionic liquids therefore represent an interesting material for investigation in this context.

4.2.3   Electrolyte: Organic Solvent and/or Ionic Liquid

A non-aqueous electrochemical process necessarily requires a non-aqueous electrolyte. We consider two broad classes of solvents that may be suitable for the system under consideration: polar
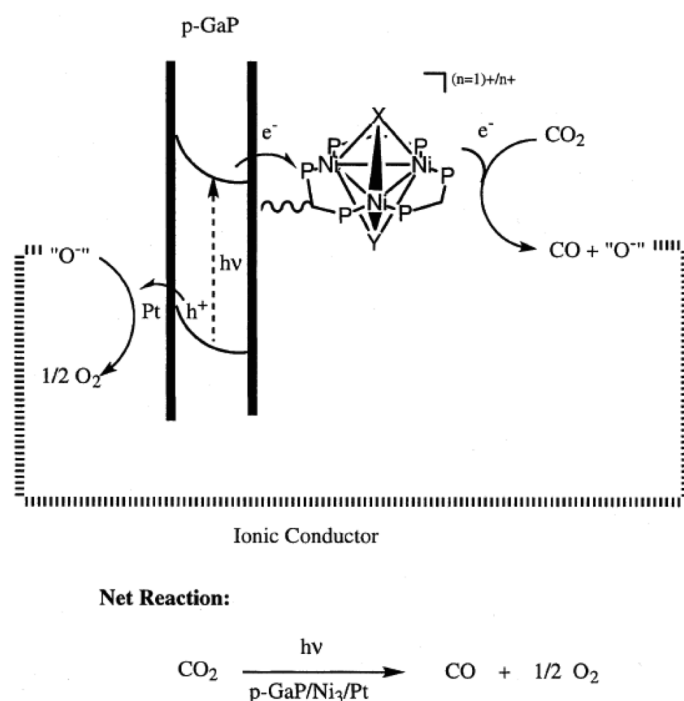
Figure 4.4: A semiconductor PEC system for the CO_2 splitting. Adapted from *Breedlove et al.* (2001).

organic solvents and ionic liquids. The majority of the non-aqueous CO_2 electrochemistry work described in the literature is performed in acetonitrile solvent at 25°C and 1 bar CO_2 pressure. This may not be ideal for a broad range of operation on Mars, as acetonitrile freezes at −44°C and does not dissolve significant quantities of CO_2 or metal carbonate species (*Fogg*, 1992). In contrast, certain ionic liquids are known that have a much wider liquid range, could offer solubility for metal carbonates, and may also dissolve CO_2 to a greater extent (*Zhang et al.*, 2009; *Lei et al.*, 2014; *Seo et al.*, 2014). However, these materials are much more viscous than organic solvents, so it is likely that a mixture of ionic liquids and organic solvents would be required to offer the full range of desirable electrolyte properties: i) wide liquid range (down to the lower limit of Mars operating temperatures); ii) wide voltage window (suitable for both cathode and anode processes); iii) low viscosity to enable reasonable electrode kinetics under operating conditions and iv) solubility for reactant species (CO_2, CO_3^{2-}). Table 4.1 identifies suitable materials for investigation in this context:

4.2.4 Membrane: Porous Material for Carbonate Transport

Membranes have several potential applications in water-free CO_2 reduction systems. Anion-conducting, gas-blocking membranes are needed as separators of the anode and cathode com-

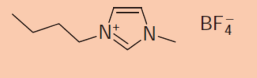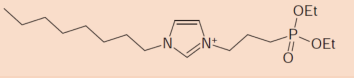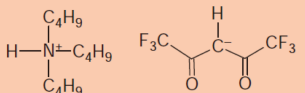| Solvent	Melting point / °C	Boiling point / °C	Viscosity (25 °C) / cp	Voltage window (est.)	Estimated potential for CO_2 and CO_3^{2-} solubility
Acetonitrile	-44	81	0.3	6.3	Poor
Tetrahydrofuran	-108	66	0.5	5.3	Poor
Dichloromethane	-97	40	0.4	5.0	Very Poor
Methyl acetate	-98	57	0.4	5.1	Poor
Dimethylformamide	-60	152	0.9	5.5	Poor
Nitromethane	-90	115	0.7	4.2	Poor
Diethyl carbonate	-74	127	0.7	6.7	Very Poor
Tetrahydrothiophene	-96	119	0.6	7.0	Poor
$[BMIM][BF_4]$	-82	n/a	120	4.7	Good
$[DPPOIM][PF_6]$	-93	n/a	200	4.7	Good
$[N444H][(CF_3CO)_2CH]$	-92	n/a	20	4.0	Good

Table 4.1: Organic solvents and ionic liquids with promise as non-aqueous solvents for low-temperature CO_2 and CO_3^{2-} electrochemistry.

partments in devices with liquid electrolytes. Anion-conducting, gas-permeable membranes are needed to host catalysts in gas-diffusion electrode (GDE) configurations. Although membranes are an energy-efficient means of separating gas mixtures, CO and O_2 are too similar in their properties for membranes to be useful in this application, particularly because allowable levels are about 1 ppm in room temperature air. Current technology for removal of CO from gas streams is mature and involves catalytic oxidation (*Twigg*, 2007).

Although physically different because of their applications, anion-conducting membranes must have the conductivity and gas permeability/blocking properties required for their applications. They must be compatible with the non-aqueous electrolyte, catalyst (for GDEs), and gaseous products, as well as electrochemical processes. The properties of the membranes must be stable in use for at least 4–6 years over the temperature range experienced in the Martian environment. They must be mechanically robust to space travel and ground transport on the Mars surface. A high TRL level is necessary for near-term testing and deployment. There are currently no known commercially available anion-conducting membranes that have been evaluated under conditions expected for non-aqueous CO_2 reduction systems (*Varcoe et al.*, 2014). R&D is needed to identify

suitable materials and demonstrate their performance. Key considerations are discussed in the rest of this section.

Membrane material. There are 3 classes of membranes (*Freeman et al.*, 2006). Inorganic porous materials, which function by sieving gases according to size to separate mixtures, have high performance and are very stable but mechanically fragile. Polymers effect separation by differential permeation, where different components of a mixture can have distinct solubility or diffusivity through the polymer. Polymeric materials can have good mechanical properties, but their transport properties are sensitive to their preparation and environment, and performance can vary with time. Hybrid materials, which are composites of polymers and inorganic grains, can have optimized properties—good stability, separation, and mechanical characteristics—but are at a very early stage in their development. Because only polymer-containing membranes can incorporate anion diffusion paths, they are the only option for nonaqueous CO_2 reduction.

Optimum ionic conductivity and gas permeability properties. Available ion-conducting membranes have been developed for high current applications (*Varcoe et al.*, 2014). A computational modeling study of requirements for membranes in aqueous PEC systems has shown that the membrane properties that result in high conductivity also result in product crossover because of the structure of the ion-conducting channels (*Berger et al.*, 2014). Product crossover results in back reactions that reduce efficiency, as well as contamination of the product gas streams. This is of particular concern for CO contamination of O_2 because of the demand placed on cleanup technologies. The modeling work revealed that a reduction in conductivity to accommodate currents typical of PEC devices (10s of mA rather than ~1 A) results in a significant reduction in product crossover, providing criteria for membrane optimization.

Chemical compatibility and stable conductivity. The chief concern for the performance stability of polymeric membranes used in the presence of CO_2 is plasticization, which increases permeability over time (*Horn & Paul*, 2011). Thick and thin membranes have different responses, and trends in permeability over time are complex. Research on CO_2 separation from gas mixtures has revealed routes to stabilization of membrane performance (*Wang et al.*, 2016). Studies of anion-conducting membranes for fuel cell applications have reported some data on electrochemical stability (*Merle et al.*, 2011). These are important factors to consider; however, their applicability to non-aqueous CO_2 reduction devices, whether liquid electrolyte-based or involving gas diffusion, is unknown.

Stable permeability in use for 4–6 years over the temperature range expected on Mars. Membrane permeability can be affected by two types of changes in mechanical properties: aging of the structure of the membrane matrix, which is usually synthesized far from equilibrium, and fracture. Both processes are affected by temperature. The average temperature on Mars is 210 K, spanning a roughly ± 90 K range depending on latitude, time of day, height above the surface, and time of year. As temperature increases and decreases, all materials in the PEC cell will expand and contract according to their thermal coefficients of expansion. Polymers can vary widely in response to thermal swings depending on their internal morphology. They will densify to some degree because of relaxation of the molecular chains, directly reducing their permeability (*Murphy et al.*, 2011; *Huang & Paul*, 2004). This effect is counterbalanced by plasticization as described above, but cannot be neutralized. Although polymers are generally less brittle than inorganic materials, if temperature variations are accompanied by significant density changes or phase changes, the differential coefficients of thermal expansion of the membrane and materials in contact with it can cause the membrane material to develop cracks, allowing electrolyte leakage and mixtures that should be separated to pass through unchanged. The mechanical properties of polymer-based membranes must be carefully matched to those of their framing and mounting materials. The remedy is precise temperature control of CO_2 reduction cells both in use and at rest by incorporating stored heat capabilities or separate heaters into the design of the units.
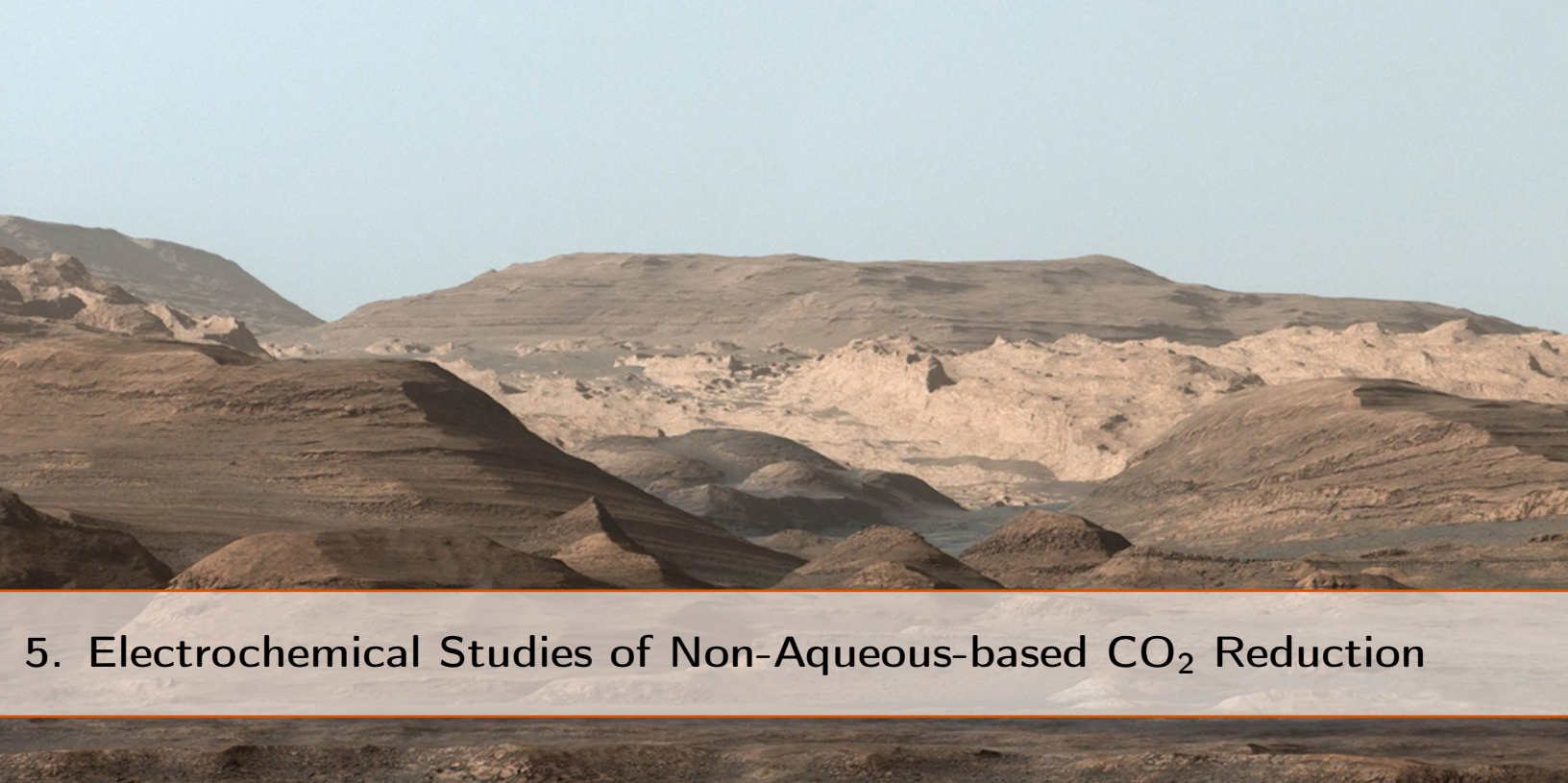
5. Electrochemical Studies of Non-Aqueous-based CO$_2$ Reduction

As noted above, given the challenges of mining, transporting, purifying, and delivering water from Mars resources to a PEC or EC reactor system, the non-aqueous-based CO$_2$ reduction system is perhaps the first logical step toward implementing an efficient low-temperature oxygen generation scheme. In this section, we describe some preliminary experimental work at JPL to assess the viability of the reaction pathway operating at low temperatures relative to SOXE approaches.

5.1 Fundamental Electrochemistry

A recent report (*Sampson & Kubiak*, 2016) described reductive dimerization of CO$_2$, generating CO and CO$_3{}^{2-}$ as products according to Process A (Equation 5.1):

$$2\,CO_2 + 2\,e^- \longrightarrow CO + CO_3{}^{2-} \qquad\qquad \text{(5.1, Process A)}$$

This offers a potentially efficient means for converting CO$_2$ into useful products, which could be useful in the context of Mars ISRU if the by-product CO$_3{}^{2-}$ could be oxidized into O$_2$ according to Process B (Equation 5.2):

$$CO_3{}^{2-} \longrightarrow \tfrac{1}{2}\,O_2 + CO_2 + 2\,e^- \qquad\qquad \text{(5.2, Process B)}$$
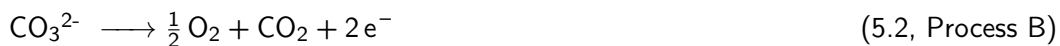
That is, a full electrolysis cell could be envisaged whereby Process A occurs at the cathode (generating CO, which could be used as low-grade fuel) and CO$_3{}^{2-}$ is transported via an anion-exchange membrane (as known for fuel cell technologies; *Vega et al.*, 2010) to the anode, where it is converted to O$_2$ via Process B (with concomitant release of CO$_2$). Hence, the work described

below focuses on characterizing both reactions in solvents of interest (MeCN, ionic liquids) and conditions relevant to Mars operation.

5.2   Experimental Approach

CO_2 reduction (Process A) and O_2-evolution (Process B) reactions were evaluated separately using pressurized stainless steel Swagelok cells fitted with pressure sensors (see Figure 5.1 for their configuration). All manipulations were carried out under anhydrous conditions, using anhydrous materials. Coated electrodes were prepared at JPL or obtained from commercial partners. Mg metal, magnesium triflate ($Mg(OTf)_2$), lithium carbonate, sodium carbonate, cesium carbonate, trimethylneo-pentylammonium fluoride, lithium peroxide, tetrabutylammonium hexafluorophosphate, acetonitrile (MeCN) and N,N'-dimethylacetamide (DMA) were supplied by Aldrich. 1-Ethyl-3-methylimidazolium tetrafluoroborate, 1-ethyl-3-methylimidazolium triflate, 1-ethyl-3-methylimidazolium bis(trifluoromethylsulfonyl)imide, butyltrimethylammonium bis(trifluoromethylsulfonyl)imide (BTMA-TFSI), diethylmethylammonium triflate (DEMA-OTf), and choline bis(trifluoromethylsulfonyl)imide ionic liquids were supplied by Iolitec. $Mn(6,6'$-dimesityl-2,2'-bipyridine)$(CO)_3(MeCN)(OTf)$ catalyst was supplied by the Kubiak group at UCSD. Differential electrochemical mass spectrometry (DEMS) was performed using an SRS Residual Gas Analyzer connected to a Pfeiffer turbomolecular pump, for which access was generously provided by Liox Power, Pasadena, CA. Electrochemical experiments were carried out using a BioLogic system. Experiments were carried out in a Tenney thermal chamber (Process A) or in a Binder oven at 30°C (Process B), after at least 2 hours of thermal equilibration.
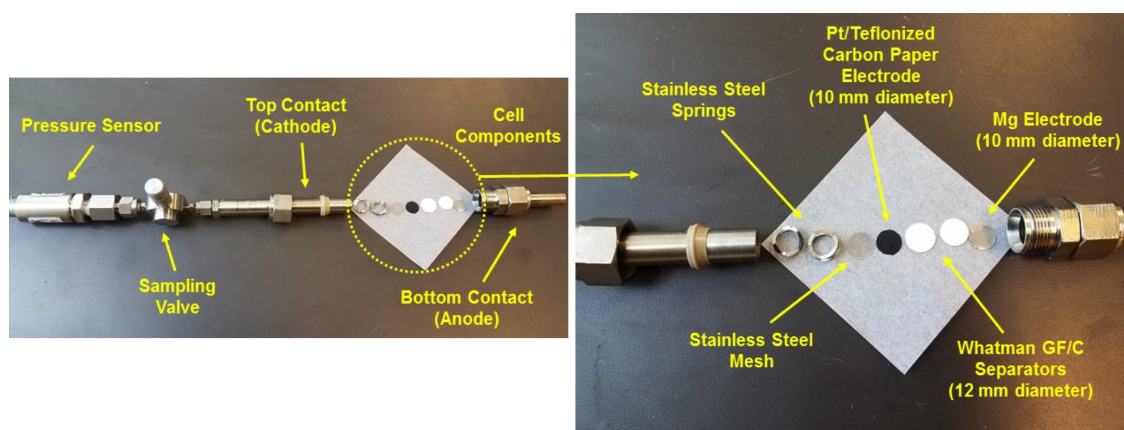
Figure 5.1: Stainless steel Swagelok cells fitted with pressure sensors (left) used for electrochemical experiments, shown with cell components for CO_2 reduction (right).

For Process A, the electrodes used were either Pt/Teflonized carbon paper or Mg metal. The electrolyte (~100 µL per cell) comprised 0.1 M $Mg(OTf)_2$ and 0.5 mM $Mn(6,6'$-dimesityl-2,2'-bipyridine)$(CO)_3(MeCN)(OTf)$ catalyst dissolved in MeCN/0.1 M tetrabutylammonium

hexafluorophosphate (TBA-HFP) or ionic liquid solvent. Cells were assembled, evacuated to 0.01 psi pressure, and then back-filled with CO_2 ("bone dry" grade) to the appropriate pressure. This evacuation/back-filling process was repeated for a total of five cycles. For Process B, the electrodes used were either carbon-based active material (free-standing film or coated onto Al foil), lithium titanium oxide (LTO) coated onto Al foil, or Pt/Teflonized carbon paper (all cells tested were symmetric). The electrolyte comprised a saturated solution of carbonate salt (Li, Na or Cs) in ionic liquid, in some cases containing 0.1 M trimethylneo-pentylammonium fluoride in an attempt to improve carbonate solubility. Cells were assembled, evacuated to 0.01 psi pressure, and then back-filled with Ar ("Ultra High Purity" grade) to the appropriate pressure, again for five evacuate/back-fill cycles. Cells were analyzed by DEMS before electrolysis, then connected to the BioLogic instrument for the prescribed experiments, and subsequently analyzed by DEMS following equilibration for at least one hour at room temperature after electrochemical testing.
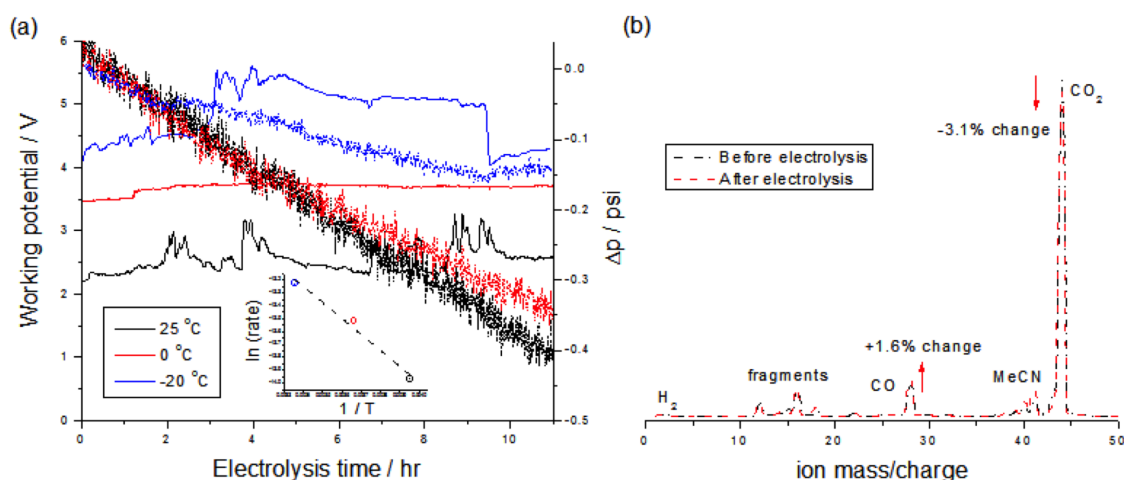
Figure 5.2: (a) Summary of CO_2 reduction experiments showing working potential (left) and observed pressure change (right) as a function of electrolysis time and temperature, at 50 µA in MeCN. The bottom inset plot reveals Arrhenius behavior of the reaction from +25 to −20°C. (b) Representative DEMS data for CO_2 reduction in MeCN at 0°C. Note that CO is a fragment ion of CO_2 (hence, always observed regardless of CO concentration in a CO_2 atmosphere); therefore, changes in gas-phase CO concentration are determined quantitatively by comparing the ratios of CO and CO_2 peaks before and after electrolysis.

5.3 Process A: Reductive Dimerization of CO_2 to CO and CO_3^{2-}

Literature investigations (*Sampson & Kubiak*, 2016) utilized an air-tight 3-electrode setup under 1 atm CO_2 with glassy carbon working electrode, Ag/AgCl reference electrode, and Mg counter electrode (which behaves as a sacrificial electrode, providing Mg^{2+} to solution as $MgCO_3$ precipitates during CO_2 reduction); electrolysis was carried out at a constant potential of ~2.1 V

vs. Li$^+$/Li, with stable current density of ~1 mA/cm^2 observed over 6 hours. Tests described here attempted to translate this setup to a 2-electrode pressurized Swagelok cell, with Pt/Teflonized carbon paper working electrode (cathode) and Mg anode. In this configuration, the inclusion of a reference electrode was not possible, so electrolysis was carried out under constant current and the working potential allowed to drift throughout the experiment; a low current density of ~0.06 mA/cm^2 was chosen so as not to stress the cells kinetically in these proof-of-concept studies. Representative experimental data are shown in Figure 5.1; CO$_2$ reduction was observed under a range of conditions, confirmed by mass spectrometry (Figure 2) and quantitative analysis was carried out by evaluating the in-situ pressure change assuming ideal gas behavior and the stoichiometry of Equation 5.1 (summarized in Table 5.1 below, at 1 atm CO$_2$):

Electrodes	Electrolyte solvent	Temperature / K	Average working potential at 50 µA / V	CO$_2$ reduction rate / mol hr^{-1}	Faradaic efficiency (FE) / %
Pt/C cathode, Mg anode	MeCN	298	2.55	1.8×10^{-6}	94
Pt/C cathode, Mg anode	MeCN	273	3.69	1.3×10^{-6}	70
Pt/C cathode, Mg anode	MeCN	253	4.85	8.6×10^{-7}	46
Pt/C cathode, Mg anode	BTMA-TFSI	298	5.16	1.6×10^{-6}	88
Mg cathode, Mg anode	MeCN	298	0.90	4.6×10^{-7}	25
Pt/C cathode, Mg anode	MeCN, no catalyst	298	2.82	1.4×10^{-7}	7

Table 5.1: Summary of CO$_2$ reduction experiments under 1 atm CO$_2$. Electrolytes contained 0.1 M Mg(OTf)$_2$ and 0.5 mM catalyst (unless stated otherwise); MeCN also included 0.1 M TBA-HFP.

The reaction represented by Equation 5.1 appears to proceed well at 298 K under similar conditions to those described by described by the Kubiak group (cf. *Ratiff et al.*, 1986–1988; *Lewis*, 1993) (they report a FE of 98±3%; *Sampson & Kubiak*, 2016). A small degree of H$_2$ evolution was also evident in the DEMS data, but typical H$_2$ concentrations observed were <1% of the total gas volume so this is not considered significant and presumably corresponds to less-than-perfectly anhydrous conditions. Variable-temperature experiments in MeCN suggest Arrhenius behavior down to –20°C, with decreasing FE and increasing overpotential as the temperature decreases. Interestingly, at 298 K reduction of CO$_2$ occurs at similar rates in MeCN and BMTA-TFSI ionic liquid (although at greater overpotential in the ionic liquid); low-temperature experiments were unsuccessful for BMTA-TFSI as the pure liquid freezes at ~7°C. It was noted that the catalyst appears more stable in ionic liquid solution (by eye, discoloring in MeCN over a period of hours while persisting in BMTA-TFSI for several days). The catalytic effects of both Pt electrode and solution-phase catalyst are readily evident from Table 5.1, and this suggests that productive efforts can be made to optimize these materials in future work.

Variable-pressure investigations were also carried out (at 0.1 psi CO_2, 298 K). Unfortunately, a pressure increase was observed during the experiments (inconsistent with Equation 5.1) using either MeCN or BMTA-TFSI solvent; this is attributed to electrolyte decomposition occurring (generating H_2) instead of CO_2 reduction, suggesting that the concentration of CO_2 in electrolyte solution is not sufficient for catalytic reaction at this lower pressure.

Tafel experiments (at 50 μV/s) on Pt/C-Mg cells with MeCN electrolyte at 298 K indicated this cell configuration could operate at around ~0.6 mA/cm^2 before significant non-linear overpotential response (i.e., about twice the current density used in the CO_2 reduction experiments described here, roughly consistent with the electrolysis current density observed for constant potential electrolysis in the different cell configuration used in the literature).

5.4 Process B: Oxidation of CO_3^{2-} to O_2 and CO_2

In order for O_2 generation to occur as anticipated by Equation 5.1, an anhydrous source of CO_3^{2-} ions in solution is required (as, presumably, water oxidation will take preference in aqueous systems). This is not a trivial pre-requisite as simple carbonate salts are only sparingly soluble in common organic solvents (e.g., MeCN). Initial efforts therefore focused on screening ionic liquids with carbonate salts of lithium, sodium and cesium. In general, solubility of these salts appeared to be less than 0.1 M in all ionic liquids attempted and did not vary much with the cation, despite reports in the literature of high solubility for Cs_2CO_3 in certain ionic liquids (*Jorapur & Chi*, 2005). Solubility was notably increased for Li_2CO_3 (although still saturated around 0.1 M) upon addition of around 0.1 M trimethylneo-pentylammonium fluoride, suggesting that the salt metathesis product (i.e., trimethylneo-pentylammonium carbonate) has higher solubility than the alkali salt. Hence, ammonium carbonates might be a better choice as a carbonate source (and, hence, alkylammonium cations as spectator ions in a full electrochemical cell), however these are not readily available commercially. In general, linear alkylammonium-containing ionic liquids (i.e., BTMA-TFSI and DEMA-OTf) had greater solubility for carbonate salts than those with cyclic cations; DEMA-OTf (with an N-H containing cation) displayed the greatest solubility behavior of all, potentially indicating a preferential interaction between this H-bond donor cation and the CO_3^{2-} anion. An alternative ionic liquid incorporating the choline cation (with a pendant O-H group) was investigated in this context and did, indeed, appear to have similarly improved solvating properties. However, the relatively high melting point (20°C) limits its practical use as a solvent, thus requiring blending with DMA for testing. Carbon and LTO electrode exhibited poor wetting with BTMA-TFSI solvent so this was blended with MeCN for testing. Attempted O_2-evolution cell tests are summarized in Table 5.2 below.

Electrodes	Electrolyte solvent	Electrolyte salt	Major product	Gas evolution details
Graphite (foil)	BTMA-TFSI/MeCN	Li_2CO_3	Trace H_2	
Activated carbon (foil)	BTMA-TFSI/MeCN	Li_2CO_3	Trace H_2	
Activated carbon (film)	BTMA-TFSI/MeCN	Li_2CO_3	Trace H_2	
LTO	BTMA-TFSI/MeCN	Li_2CO_3	H_2	$\sim 1 \times 10^{-6}$ mol hr^{-1} (H_2)
Pt/C	BTMA-TFSI	Li_2CO_3	Trace O_2	$< 1 \times 10^{-7}$ mol hr^{-1} (O_2), ~50% p_{O_2} increase
Pt/C	BTMA-TFSI	Cs_2CO_3	Trace O_2	$< 1 \times 10^{-7}$ mol hr^{-1} (O_2), ~10% p_{O_2} increase
Pt/C	DEMA-OTf	Li_2CO_3	CO_2, trace O_2	$< 1 \times 10^{-7}$ mol hr^{-1} (CO_2), ~2% p_{O_2} increase
Pt/C	DEMA-OTf	Cs_2CO_3	CO_2, trace O_2	$< 1 \times 10^{-7}$ mol hr^{-1} (CO_2), ~1% p_{O_2} increase
Pt/C	Choline-TFSI/DMA	Li_2CO_3	H_2, CO_2	$\sim 1 \times 10^{-7}$ mol hr^{-1} (H_2, CO_2)
Pt/C	DMA	Li_2O_2	O_2	$\sim 1 \times 10^{-6}$ mol hr^{-1} (O_2), ~2500% p_{O_2} increase

Table 5.2: Summary of O_2 evolution tests under Ar at 303 K. Electrolytes contained ~0.1 M salt. Cells were electrolyzed for a number of hours at current density ~0.03 mA/cm^2.

5.5   Significance of Results

(i) Electrocatalytic reduction of CO_2 can be effected through homogeneous catalysis at temperatures as low as –20°C under 1 atm CO_2, with good FEs. Experimental current densities are low at present (~3 orders of magnitude below those achievable in high temperature SOXE processes, making direct estimates of rates of eventual CO_2 production capability meaningless at this stage; *Hecht*, 2016) but these should be improved significantly in future work through modification of electrode, electrolyte, and catalyst composition, as well as improvements in cell design. This will enable the potential operational energy savings possible through low-temperature electrocatalytic ISRU to be evaluated in a more properly-optimized cell setup.

(ii) O_2 evolution from CO_3^{2-} ion in ionic liquid media is slow and inefficient, so future designs for full electrocatalytic ISRU cells should investigate alternative anode reactions and charge carriers.

Hence, further studies of low-temperature alternatives to SOXE ISRU processes for O_2 and fuel generation on Mars are warranted based on the proof-of-concept CO_2 reduction experiments described herein.
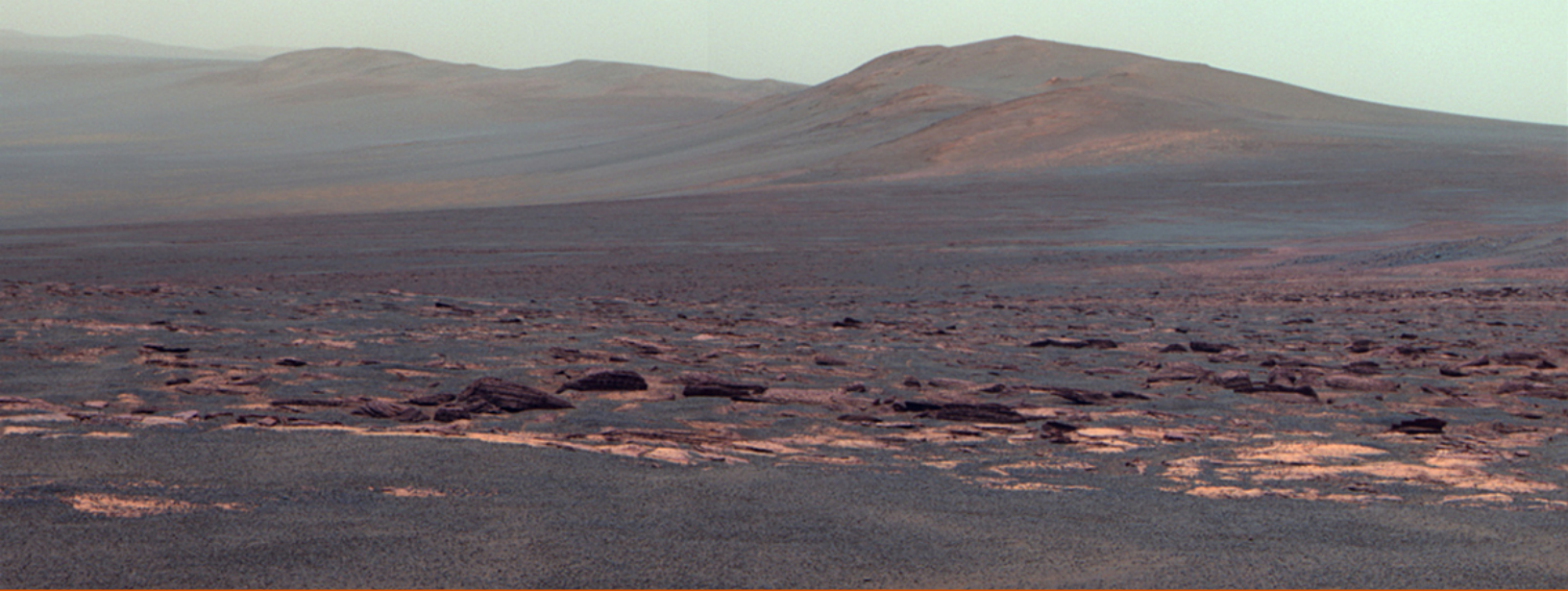
6. System-Level Considerations

The following sections describe various aspects at the system- and sub-system-level considerations for EC- or PEC-based oxygen and fuel generator stations operating on Mars. In some sections, only case-specific applications are considered, e.g., only non-aqueous PEC systems.

6.1   Oxygen Calculations: Needs and Production

Of course, oxygen gas is one of the crucial components for the human life support system on Mars. A large amount of oxygen is also required for the propellant combustion in the Mars Ascent Vehicle (MAV). In this section, the basic requirements for oxygen production by the non-aqueous PEC device and its comparison to the MOXIE device are discussed. These requirements are based on a mission timeline of 480 days (16 months), excluding 10 months of transit and margin time. Oxygen gas needs to be liquefied to minimize storage volume.

Average space crew consumption and accommodation have been defined by various sources, including the ISS program, Environmental Control Systems at JSC, Advanced Exploration System's Logistics Repurpose and Reuse project, and the Human Spaceflight Architecture Team (HAT). Table 6.1 below summarizes water and oxygen requirements for the Orion Multi-Purpose Crew Vehicle. According to this data, one crew member will require 0.82 kg of oxygen per day (*Drake et al.*, 2010). The total amount of oxygen needed for 5 people for the 480-days-long Mars mission is equal to 1968 kg.

According to the M-WIP (Mars Water ISRU Planning) study by the SMD/Mars Program office, the propellant for the MAV will require 24.6 metric tons of oxygen (*Muscatello & Santiago-*

Assumptions	Unit	Value
Oxygen Metabolic	kg per crewday	0.82
Water – Drink	kg per crewday	2
Water – Food Rehydration	kg per crewday	0.5
Water – Medical	kg per crewday	0.05
Water – Hygiene	kg per crewday	0.4
Water – Flush	kg per day	0.25
Cabin Air Leakage	kg per day per module	0.00454
Cabin Air Leakage – Orion	kg per day	0.00908

Table 6.1: Gas and Liquid Assumptions

Maldonado, 2012). 78% of MAV propellant is oxygen, which represents 55% of the return vehicle mass. Another study of the MAV propellant mass shows a similar value of 22.7 mT (*Muscatello et al.*, 2016).

Scenario	Propellant-related S/C Mass (mT)					Propellant Produced (mT)	Figures of Merit (n:1)		Other Considerations		
	ISRU h/w	O_2	CH_4	Total	Mass Savings		Mass savings: ISRU h/w mass	Production: ISRU-related s/c mass	Requires excavation?	Constrains landing site?	Flight-like prototype?
No ISRU	0	24.6	7	31.6		0					
LOx only	1	0	7	8	24	24.6	24	3	No	No	Yes
LOx + CH_4	1.7	0	0	1.7	30	31.6	18	19	Yes	Yes	No

Table 6.2: Propellant Requirements by Scenario

Oxygen consumption during EVA lasts for 8 hours and, with an oxygen contingency of 45 min for one activity, is equal to 0.72 kg (*Drake et al.*, 2010). Considering one activity per day per person, the overall oxygen needed for 5 people for the mission is conservatively estimated to be 1728 kg.

The total oxygen requirement including human support, MAV propellant, and EVA is 28.3 mT, and therefore a continuous production of 2.46 kg/hr of oxygen is required.

Considering the ISRU strategy, as opposed to sourcing the oxygen from Earth, oxygen can be produced from carbon dioxide, the major component of Martian atmosphere (>95%), or electrolysis of sub-surface water. Due to the complexity, site dependency, and mission risk currently associated with using water resources on Mars, utilization of atmospheric CO_2 with no dependency on latitude is deemed the preferred way to produce oxygen. In this section, we describe a non-aqueous PEC device to convert CO_2 to O_2 and CO by the following reaction:

$$CO_2 \longrightarrow CO + \tfrac{1}{2}O_2 \text{ (4e}^- \text{ process with Nernstian potential 1.33 V)}$$
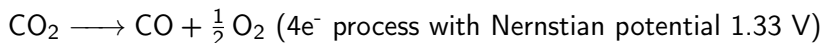
In the MOXIE system, oxygen is generated via carbon dioxide electrolysis at 800°C in a solid oxide electrolyzer. The most obvious difference between the PEC approach and MOXIE is that the PEC device can potentially operate at much lower temperatures than MOXIE. Solid oxide electrolysis usually requires energy input of 25–35 kW (to produce 2.2 kg O_2/hour) for electrolysis current and heat.

For a production rate of 1 kg/h of oxygen, the non-aqueous PEC device theoretically requires

1000 g O_2 (1 mol / 32 g O_2)(4 mol e^-/mol O_2) = 125 mol e^-/h,

125 mol e^-/h (96480 C/mole e^-) = 1206,000 C/h = 335 A,

and thermodynamic power of

335 A $\times$ 1.33 V = 446 W.

Total power required for 2.2 kg/h of oxygen will range from 13–27 kW.

6.2   Deployable Structures

Each strategy discussed in this report for the in-situ generation of oxygen and fuels required for advanced robotic sample return missions or astronaut ascent from Mars requires the autonomous deployment of a lightweight structure that covers a large area on the Martian surface. For power-beaming energy from the Sun to the Martian surface in the form of microwaves as discussed below, a large structure is required, incorporating the light-gathering functions and chemical conversion elements. For aqueous or non-aqueous designs for PEC or integrated solar photovoltaic–EC processes, a light absorber component replaces the receiver on the Martian soil. A common theme among these concepts is a large-area device that can be robustly and reliably deployed to a given configuration and has feeds and collection ports for reactants and products of the electrochemical reactions, which at this time include molecules such as CO_2, O_2, CH_4, H_2O, CO, and H_2. Although each technology has other certain specific requirements, this represents the minimum needs for a structure that must be deployed on large scales on Mars.

Large deployable structures have been successfully deployed in space environments; for example, the U. S. segment of the International Space Station (ISS) includes eight unfoldable solar array wings, each measuring roughly 36 m × 12 m (*Winslow*, 1993). These wings are large, lightweight structures designed for the low-load microgravity environment in low Earth orbit. These characteristics are relevant to the power beaming application where deployment of a large solar photovoltaic array in Mars orbit is required to absorb sunlight and convert its energy into the form of microwaves that are re-radiated toward the Martian surface. A 60 m × 60 m deployable orbiting solar array and microwave energy transmitter has been designed at Caltech for use in

Earth orbit (*Arya et al.*, 2016), and should also be able to be leveraged for deployment in Mars orbit.

However, similar-sized structures have not been deployed on the surface of celestial bodies, e.g., Earth's moon or Mars, where gravitational loading dominates (roughly 0.4 g or 3.71 m/s^2 on the Martian surface). The largest solar array deployed on the Martian surface was for the Phoenix lander, providing roughly 3.5 m^2 of active area (*White et al.*, 2007). This is a factor of 30 smaller than the scale required for generation of oxygen and fuels required for Mars ascent. Unfortunately, the Phoenix solar array cannot be scaled up in a facile way to provide the necessary area for the present task (~900 m^2 for a rectenna array used for power beaming or up to ~120 m^2 for an integrated PEC design operating at a 10% efficiency for conversion of sunlight to methane and oxygen), and other structural architectures must be considered. Packaging and deployment represents an unresolved challenge for the realization of Martian ISRU using solar energy.

In general, uniaxial packaging and deployment—where the structure is only compacted along one axis—is easier to implement than biaxial packaging and deployment—where the extent of the structure must be reduced along two orthogonal in-plane directions (*Miura*, 1985). For this reason, when the performance of the structure depends solely on the deployed area (as in the case of photovoltaic or PEC devices) multiple independent uniaxially compacted structures are often used, as opposed to a single larger biaxially compacted structure. When area continuity of the deployed structure is required, as in the deployment of the rectenna for the power beaming architecture, biaxial packaging and deployment techniques must be employed; this often results in engineering complexity. Typical uniaxial folding motifs include fan folding (e.g., in the Phoenix solar array), z-folding (e.g., in the ISS solar array wings), or rolling (e.g., in the second generation Hubble solar array). Key drivers for the structural design include deployed area, deployed shape accuracy, maximum allowable deflections, and dominant loading conditions.

The first two motifs, i.e., fan folding and z-folding, require sharp geometrical kinks in the structure; these kinks can be implemented either using hinges (e.g., piano hinges as on the ISS solar array wings) or shallow curves that limit the minimum radius of curvature of the material being folded. Creases, i.e., concentrated bending stresses, should be avoided to prevent creep, plasticity, damage, and non-planarity when deployed (*Papa & Pellegrino*, 2008). (Note that this is a general design principle and may be forsaken in cases where avoiding creases adds complexity and the material system is proven to be robust under creasing loads, e.g., the edges of the ISS solar array wings, which are used for power routing and are designed to be folded and unfolded for many tens of cycles.) At this time, rolling appears to be a promising candidate for the folding architecture of the proposed Mars ISRU designs. Rolling limits the maximum bending stresses imposed on the structure during packaging without the need for mechanical hinges and without sacrificing packaging efficiency. Back-rolling, also known as curvature reversals, can be used to reduce shear stresses that occur during the rolling of long sheets of laminated materials (*Arya et al.*, 2016).

Deployment may be driven by inflation with fluid working against the 600 Pa pressure at the Martian surface, by an unfoldable structural framework, or by external independent robots. It may even be advisable to incorporate the ability to deploy and retract the structure at night to help with thermal management due to non-radiative emission from the high-surface-area materials. However, note that to require a deployable space structure to be retractable, and to be able to retract and deploy over hundreds, if not thousands, of cycles without maintenance, adds immense complexity to the design and testing of such a system.

Based on the discussion above, three preliminary packaging and structural architectural concepts were developed. These are illustrated below, and are offered as strawmen concepts.
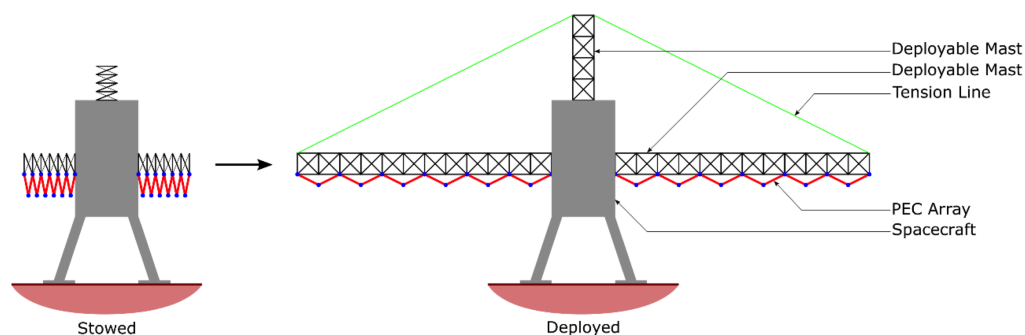

Figure 6.1: Z-Folded, Mast-Supported PEC Array

The first concept is illustrated in Figure 6.1, which uses z-folding to package the array, and a deployable mast (*Mikulas et al.*, 2006) to hold the array off the ground. The z-folds are represented here as mechanical hinges. One mast and one z-folded array constitute a wing. Two or four wings, arranged symmetrically about the spacecraft body, may be used to maintain structural stability, i.e., keep the overall center of gravity above the spacecraft legs. For added stiffness, tension lines connecting the ends of the wings to the spacecraft body, or the top of a shorter deployable mast, may be used. Wing widths of about 2–4 m can claim a degree of heritage from similar arrays flown in LEO (*Winslow*, 1993). If four wings are used, the wing lengths vary between 7.5–15 m for this range of wing widths to achieve a total deployed area of 120 m^2. These dimensions are achievable; mast lengths of up to 60 m have been achieved in microgravity environments (*Umland et al.*, 2001). Depending on the mast architecture, the array may be connected all along the length of the mast, or just at the very tips.

The second architecture, illustrated in Figure 6.2, is very similar to the first one except it uses rolling to package the array. Unlike the first concept, the array can only be connected at the tip. Initial back-of-the-envelope calculations show that for both tip-connected and continuously connected arrays, the maximum deflections of the masts are less than 10 cm over a 15 m mast length, with a mast similar to the SRTM ABLE mast architecture (*Umland et al.*, 2001).
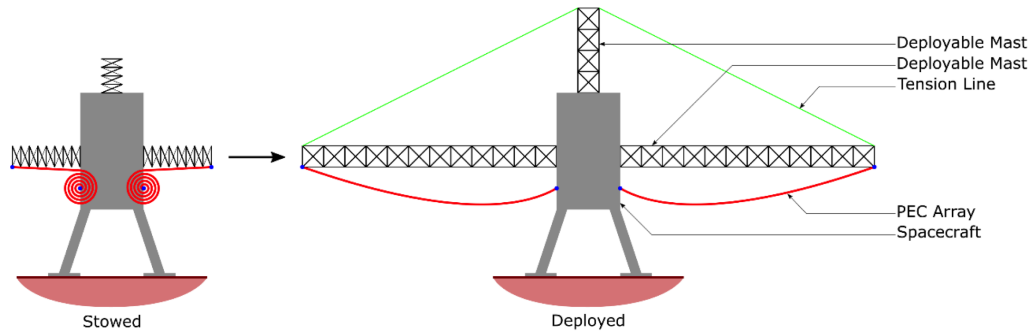
Figure 6.2: Rolled, Mast-Supported PEC Array

The last architecture, shown in Figure 6.3, addresses potential tipping concerns by adding wheeled supports at every point that is deployed out by a pantagraphic structure. The array is z-folded.

Combinations of these architectures may also yield useful designs; for instance, adding wheeled supports, or fold-out supports, at the ends of the wings in the first two concepts would increase stability and deployed structural stiffness.

Beyond packaging, deployment, and operation in gravity, there are additional challenges associated with the engineering of structures for PEC arrays. These are:

1. Device thickness: as the device thickness increases, an array with a fixed area must be packaged with greater packaging efficiency into a limited fixed volume envelope;

2. Pressure differential: the structure must be able to sustain the pressure of the fluids contained within the PEC while limiting leaks; and

Figure 6.3: Z-Folded, Pantagraph-Supported PEC Array

3. Optical transparency: the top structural layer of the PEC array must be transparent, which limits materials choices.

The design and engineering of the array itself is a challenge. We list three possible architectures for the array:

Venetian blind structure. This structure was presented conceptually for PEC applications in the late 1970s (*Gerischer*, 1979), but was recently more completely engineered and demonstrated 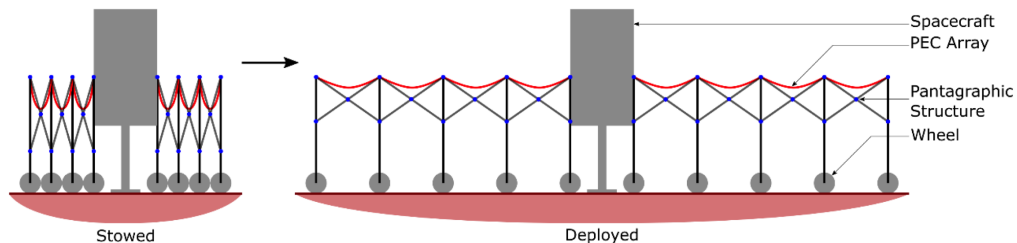by the Joint Center for Artificial Photosynthesis (JCAP) in a practical prototype for sunlight-to-chemical energy conversion at >10% efficiency. The advantage of this design is that the light absorption area is not shaded by the electrolyte and/or electrocatalysis area and the two regions can be independently sized to afford the optimum performance given the inputs. A major challenge with this design is that edges of functional materials must be bonded to one another and not form regions of weakness in the overall design, which they likely will.

Monolithic structure. This structure includes slight modifications of the Venetian blind structure, most notably where the materials are fabricated from a single monolithic base support material (see Figure 6.4 below). The advantage of this design is that regions of high stress and/or large radii of curvature in the device structure consist of one continuous piece of material; moreover, this design obviates challenges with differences in materials properties, e.g., thermal expansion coefficient, thermal conductivity, modulus. In principle, such a system could be made flexible to allow inflation of the baffles for deployment. A major challenge with this design is that one base material must be lightweight and both ionically and electrically conductive depending on desired properties at each location.

Rectenna receiver structure. This structure is a subset of the monolithic structure, but requires less complexity. Instead of incorporating integrated light absorbers and electrocatalysts, this design only requires a wireframe receiver dipole antenna (rectenna) with incorporated electrocatalysts, and thus also relaxes the optical transmission properties required of the plastic encapsulation. The functional materials must be connected to electronic circuits, either integrated or separately, to impart rectification in the AC microwave electric field such that there is a DC current output to drive the electrocatalytic reactions, but this is straightforward and is not expected to affect deployment. The microwave receiver likely cannot be placed under the electrolytic components because microwave power is attenuated by free charge carriers including ions in the electrolytes used in the electrochemical cells (*Infelta et al.*, 1977).

KEY
Solar Cell, **Catalyst Layer**, **Electronically conductive substrate**, **Ionically conductive membrane separator**, **Robust and gas impermeable containment**

"Nafion"

"Nafion(prime)"
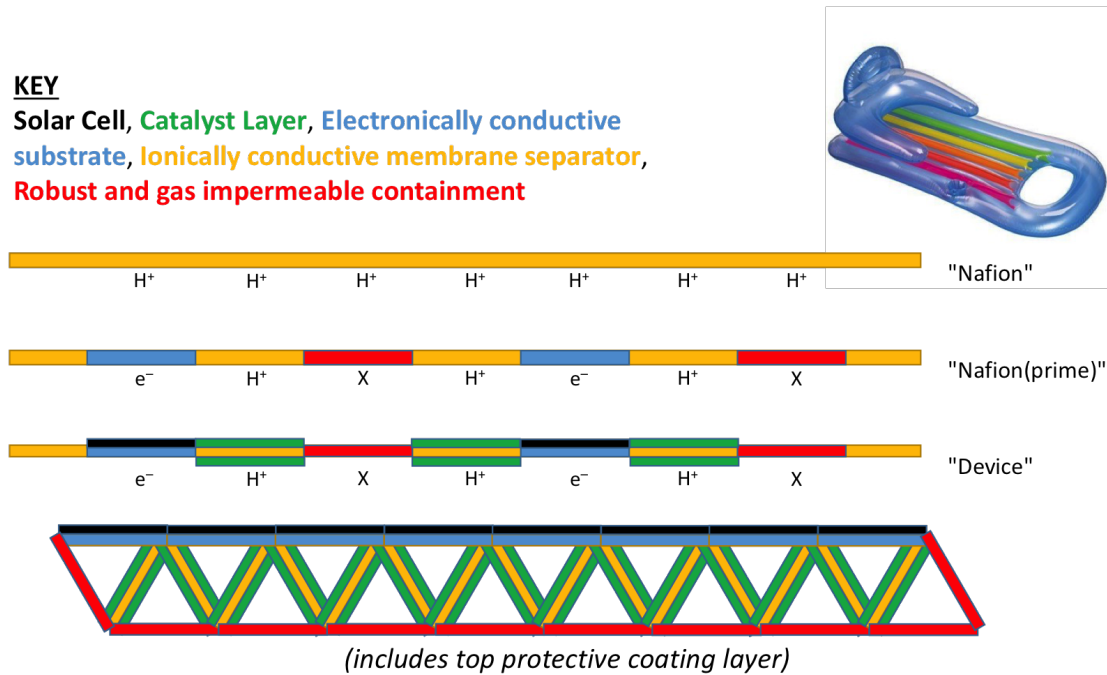
"Device"

(includes top protective coating layer)

Figure 6.4: Monolithic deployable structure variant of the Venetian blind structure, akin to an inflatable air mattress.

6.3 Thermal Management

In this section, thermal management of a notional PEC system is considered, with rough order-of-magnitude estimates. We assume a PEC system with active area of 160 m^2 on the Martian surface. Under light dust loading, the system receives a sunlit average incident power of 556 W/m^2 throughout the Martian year, or 152 W/m^2 over the Martian sol (27% capacity factor, assuming flat plate configuration; *D. Kass*, personal communiation, 2016). With 10% of incident light lost due to reflection and/or dust, and 10% solar-to-fuel conversion efficiency, 50 W/m^2 is converted to chemical bonds, leaving 450 W/m^2 of thermal gain. We further assume 50% Faradaic efficiency for the desired product, but that is not pertinent to thermal management.

Assuming operation at 290 K, and low-emissivity coatings in the mid-infrared (~10 µm wavelength) of 5% for both top and bottom PEC surfaces, Stefan-Boltzman radiative losses are 20 W/m^2 from each surface, or 40 W/m^2 overall. Polished metal surfaces offer emissivities as low as ~3%; we assume the back surface has one of these. We also assume that a well-designed broadband coating on the top surface can achieve a similar emissivity, though the state-of-the-art is not known.

Additional thermal gain from sky and ground radiation is calculated as follows. Average mid-latitude sunlit air temperatures are assumed to be 250 K, with nighttime temperatures of 200 K.

Sky temperatures are found to be ~75 K colder than air temperatures during sunlit hours and ~40 K colder at night, at least near the Phoenix lander site (68°N; *Gendron et al.*, 2010). Although temperatures that far north are colder on average than in the mid-latitudes, we retained these rough temperature differences in calculating our overall profiles. Ground temperatures are found to track air temperatures very closely on Mars. *Gendron et al.* (2010) also report a ground emissivity coefficient of 98% (this compares with terrestrial emissivity of sand at ~75%). Martian sky emissivity was unknown; while on Earth it is ~75%, there is tremendous water vapor in the Earth's atmosphere. We assume that the thin Martian sky has an emissivity close to 1, and use 98% for consistency with the ground emissivity coefficient. As a result, the sky radiates 52 W/m^2 (sunlit) and 36 W/m^2 (night), while the ground radiates 217 W/m^2 (sunlit) and 89 W/m^2 (night). Following Kirchhoff's Law, absorption coefficients of the PEC system are equal to their emissivities at 10 μm, so these are also 5%, and overall thermal gain of the panel is 27 W/m^2 (sunlit) and 13 W/m^2 (night). Due to the low absorption coefficients, the sky and ground emissivities are in fact not very important; if we lowered these to 75%, the thermal gain of the PEC would be lower by only 6 W/m^2 (sunlit) or 3 W/m^2 (night).

Additional convective losses due to wind can be many times the radiative losses; we estimate this ranges from 0–2 W/m^2-K based on calculations in *Gendron et al.* (2010). Using 1 W/m^2-K as representing average conditions (wind speed ~4 m/s) for the top and bottom surfaces, total losses from both surfaces are 80 W/m^2 (sunlit) and 180 W/m^2 (night). As will be seen below, while these losses can be compensated for under normal thermal operating conditions, higher wind speeds will result in significant temperature drops that must be addressed.

	Sunlit	Night	
Incident radiation on PEC panel	400.3	0.0	W/m^2
Converted to chemical energy	−50.0	0.0	W/m^2
Remaining thermal energy	450.4	0.0	W/m^2
Radiative losses (top surface)	−20.1	−20.1	W/m^2
Radiative losses (bottom surface)	−20.1	−20.1	W/m^2
Radiative gain from sky (top)	2.6	1.8	W/m^2
Radiative gain from ground (bottom)	10.9	4.4	W/m^2
Convective losses (top surface)	−40.0	−90.0	W/m^2
Convective losses (bottom surface)	−40.0	−90.0	W/m^2
Total thermal losses	−106.6	−213.8	W/m^2
Net thermal energy balance	343.7	−213.8	W/m^2

Table 6.3: Energy balance of PEC Panel

Total losses from the PEC system are therefore approximately 107 W/m^2 (sunlit) or 214 W/m^2 (night). During sunlit hours, this still results in a significant net gain of 344 W/m^2 to be stored for release during nighttime. Assuming 10 h of full sunlight (somewhat less than half a Martian sol), there is 12.4 MJ/m^2 or 1980 MJ of gross thermal energy to be released over the 14.7 h of

the Martian night. Thermal losses are modest with insulation; we estimate that 65 MJ or 3.3% per sol is achievable with R-30 insulation (5.3 K-m^2/W).

We have investigated thermal gains from rejected heat from cryopumps maintaining liquefied CH_4 and O_2. These operate at an efficiency of ~5%. Assuming 7 t CH_4 and 28 t O_2 are being maintained at their boiling points, thermal losses from 5% emissivity spherical tanks are ~3 W, requiring a cryopump energy of ~60 W to operate. Thus, 56 W are available; we assume 80% of this quantity could be harvested for electrolyte thermal storage, or 45 W. However, this only adds 4 MJ/sol, a negligible amount.

After these storage losses and gains, there is 1919 MJ of useful energy from the PEC system to use each night to keep it warm. Spread over 14.7 h, this is a flux of 227 W/m^2, just slightly more than needed to make up for the nighttime losses of 214 W/m^2. To increase this margin of safety, a lower PEC operating temperature, higher solar absorption, and/or lower thermal emissivities would be needed.

6.3.1   Storage Tank

We assume 43 m^3 of the PEC electrolyte (modeled as H_2O) is stored in an underground tank of radius 2.2 m with a surface area of 60 m^2. Assuming R-30 insulation (5.3 K-m^2/W), thermal losses from tank to surrounding rock with an average temperature of 225 K (calculated from average of sunlit and nighttime temperatures) implies a temperature gradient of 65 K, or 732 W continuous thermal loss. Over a Martian sol, this is 65 MJ or 3.3% of stored energy, a reasonably small value. A temperature drop due to the electrolyte of 0.36 K/sol is further assumed.

During sunlit operation, assuming a PEC device layer thickness of 1 cm, a total PEC electrolyte volume is 1.6 m^3 or 3.7% of stored electrolyte volume. If the entire volume of electrolyte is circulated through the PEC system over the 10 h sunlit period, this implies a residence time of ~22 min, during which time the electrolyte temperature increases by 11.0 K. During nighttime operation, the residence time is longer (~33 min) and temperature decrease is 10.0 K due to smaller thermal losses. Subtracting the temperature drop during storage, the system is net positive by ~0.6 K/sol, implying that a small margin is available.

We have investigated the capacity of the system to store energy during a 30-sol dust storm when PEC output is reduced to essentially zero, and conclude that it is possible provided the system operates at a reduced temperature, allowing surplus thermal energy to be stored over long periods. Initial calculations indicate that lowering the operating point to 280 K would provide an excess of 57 W/m^2 during sunlit hours or 331 MJ/sol of stored energy. Over a 30-sol dust storm, a total of ~62,000 MJ would be needed to maintain PEC temperatures. However, over the 187 sols that would be required to store this thermal energy, losses would be considerable. Instead, we constrain total thermal energy loss to 50%, implying gross thermal energy of ~124,000 MJ and a

minimum duration between dust storms of 374 sols to allow the system to thermally recharge. The required volume of stored electrolyte is 2960 m^3, requiring a tank of radius 8.9 m with 996 m^2 of surface area. To achieve 50% thermal loss or 0.13%/sol therefore requires R-170 insulation (~30 K-m^2/K), or ~6$\times$ the performance of our above case (6$\times$ insulation thickness).

6.4   Power Beaming-Assisted CO_2 Reduction

As with the aqueous and non-aqueous PEC systems and EC systems described above for converting sunlight and atmospheric CO_2 to fuel and oxygen, most previous missions to Mars (with the exception of radioisotope-powered spacecraft) take advantage of incident solar energy. Presently, all of these prior missions harvest energy by way of photovoltaic arrays to power their onboard technologies. Although using ground-based solar arrays has been quite successful, there are several challenges and concerns for scaling this technology to meet the demands for much larger-scale energy conversion. One issue is the requirement to store the energy in some form for the Martian nights when no solar radiation is available. Another significant concern that has no obvious solution is mitigating the challenges from the large-area, extended-duration dust storms that occur on the planet. These storms decrease the amount of solar radiation reaching the Martian surface and the dust also covers the solar panels, making them less effective even when solar flux is high.

One interesting option that addresses many of these issues is the approach of wireless power transfer. This concept has been considered for some time for Martian and lunar missions, but has yet to be implemented. Wireless power transfer is a familiar concept, with experiments dating back to Nikola Tesla at the turn of the century. Collection of solar energy via large space-based solar arrays followed by conversion to either laser or microwave energy that is then beamed down to the planet's surface has likewise been considered before, conceptualized by Peter Glaser in the late 1960s. Shortly thereafter, experiments at the Jet Propulsion Laboratory (JPL) demonstrated over 80% conversion of beamed microwave to DC power, for a total of 30 kW DC output power transferred over a distance of 1.54 km. The Japanese Aerospace Exploration Agency (JAXA) recently demonstrated transfer of 1.8 kW to a rectenna array 55 m away, and their partner Mitsubishi has shown 10 kW over 500 m distance. JAXA has reported that they intend to implement this methodology on Earth by the 2040s. Scientists at Lawrence Livermore National Laboratory have made progress in examining the possibility of using lasers for power beaming on Earth, as lasers decrease the size requirements of the receiver relative to a microwave system. Use on Earth, however, is notably more complicated than on Mars. Possible interactions with the atmosphere, with wildlife, and with infrastructure, such as air travel, need to be considered carefully, simulated, and experimentally verified prior to use.

On the surface of Mars, these concerns are considerably lessened. An important consideration is that the significant dust storms on the planet make the use of laser light a poor choice. Losses

due to reflections lower the power that would be expected to successfully propagate to the surface during a storm. Microwaves, while more challenging to focus into a narrow beam, are expected to penetrate through these storms without significant attenuation. Furthermore, because of the closer stationary orbit position (17,000 km, versus 36,000 km on Earth), the technology should be even more feasible. A mid-level or low orbit (to less than 7,000 km) might even be acceptable. With frequencies in the range of 1–10 GHz, the electric to microwave conversion is expected to be high, conservatively on the order of 70% or more. Experiments done so far, albeit over significantly shorter distances, indicate high conversion of the beamed microwave power back into electrical energy ($>$ 80%). Further research is certainly needed to make this method succeed, but with the state-of-the art technologies combined, it appears close to reality.

One of the shortcomings of this type of power delivery is the extreme size of the solar arrays required to collect the solar energy, resulting in large mass and cost of launch and delivery. However, significant improvements have been made in deployable structures, making possible lightweight, high energy capture structures. In fact, research being done at the California Institute of Technology has resulted in the design of a deployable solar array that measures 60 m by 60 m square, with a density of only 80 g/m^2 (*Arya et al.*, 2016). Furthermore, that array was designed to be scalable such that multiple individual deployments can be attached together to make a larger structure or several separate ones can fly in constellation form. The array solar-to-electric efficiency is on the order of 30%, and research continues to advance these experimentally realized values.

On Earth, current estimates show that wireless microwave power delivery requires extremely large surface area rectenna arrays, which might make this a less attractive approach. Due to the lower orbit possibilities on Mars, the area required for the rectenna array would be $1/4$–$1/2$ the size of one required on Earth. Additionally, the coverage of the Martian surface with such an array will not carry the same concerns as on Earth, and in fact might be used to aid in the collection of feedstock, such as removal of water from the regolith. Progress has been made in all relevant areas, including conversion of electrical to microwave power, the focusing of microwave beams, and in the rectenna array receivers.

It is apparent how many variables can be modified with this design in order to accommodate the power requirements on the surface. The size of the solar array in space affects both the amount of solar energy harnessed and the resulting power beam spot size on the Martian surface; the frequency of microwaves used simultaneously affects the electric-to-microwave efficiency and the beam spot size; and the chosen orbit for the solar collector affects the power profile throughout the Martian day, as well as the spot size. Many options exist for this design and several were calculated to determine the viability of this concept. For example, assume that the solar array is put into Mars areosynchronous orbit, which can generate a continuous power supply with the appropriate targeting. Using the mass estimated for the solar array designed for use in Earth orbit, a 300-m-square array should weigh 9 mt, not including a surface rectenna and power converter.

Although this is certainly a large mass to consider sending to Mars, the appropriate comparison to make would be to the nuclear reactors that are noted in some roadmaps for providing power for Mars ISRU operations. The mass of these planned nuclear reactors to provide the requisite 26 kW is 7.8 mt to the surface. With a higher cost of mass to the surface versus mass to orbit of approximately two times, there is actually a significant saving in sending 6.6 mt to Martian orbit. A rectenna array is needed on the surface to collect the beamed power, but rough calculations estimate the mass of this array to be about 1000 kg to harness up to 50 kW of power. A commercially available microwave frequency of 94 GHz is chosen for this example; the higher frequency gives a lower (~27%) electric-to-microwave conversion but will generate a smaller spot size on the surface scaling inversely with the frequency, making it possible to send a smaller rectenna array. The microwave beam spot size is approximately 220 m square. There is a cosine latitude dependence on the power density, so $45°$ was used as a worst case scenario. At this latitude, the power density on the ground is ~50 W/m^2 (for comparison, at the equator the power density would be 71 W/m^2). While the spot size is quite large, in order to collect 50 kW (the amount to be supplied by the proposed nuclear reactors), a rectenna array of only 31.5 m square would be required (this shrinks to 26.5 m square at the equator). If we assume a mass of 20 g/m^2, the mass to surface for the rectenna would be ~20 kg, with considerable savings over the nuclear reactors.

Once the solar energy has been beamed to the surface of Mars and converted into DC electrical power by the rectenna array, this power can be used to drive the ISRU EC conversions described earlier. None of these systems have been used on a mission yet, however the technology is well-characterized, well-understood, and engineered to high Technology Readiness Level (TRL) for use on Earth. This power source could be used for any chosen EC conversion technology, such as the solid oxide conversion technology proposed on the Mars 2020 mission, MOXIE, or others. In order to consider these techniques for use on the surface of Mars, light-weighting options would be advantageous, along with environmental (such as thermal management), power, efficiency, and lifetime requirements.

Tying all of these individual pieces together into a mission to synthesize oxygen and fuels using ISRU on the surface of Mars could solve the problem of the ascent launch of a manned mission to the surface of Mars (Figure 6.5). Beyond this, a power system of this type could have significant implications for later missions. A continuous supply of power, via solar electric or chemical feedstocks, would be in place for a mission with an extended stay and eventually for a permanent base on Mars, supplying ascent and vehicle fuels and life support. More surface area rectenna array coverage can scale to up to more than 2 MW for the described solar array. Redundancy in power supply for the scientific instruments enables more flexibility and capability in science experiments. It is feasible that this power supply methodology could eventually replace other options as a primary power source for all systems, eliminating the need to deliver fuels and power supplies from Earth. While not the primary motivation, it is important to note the consequences
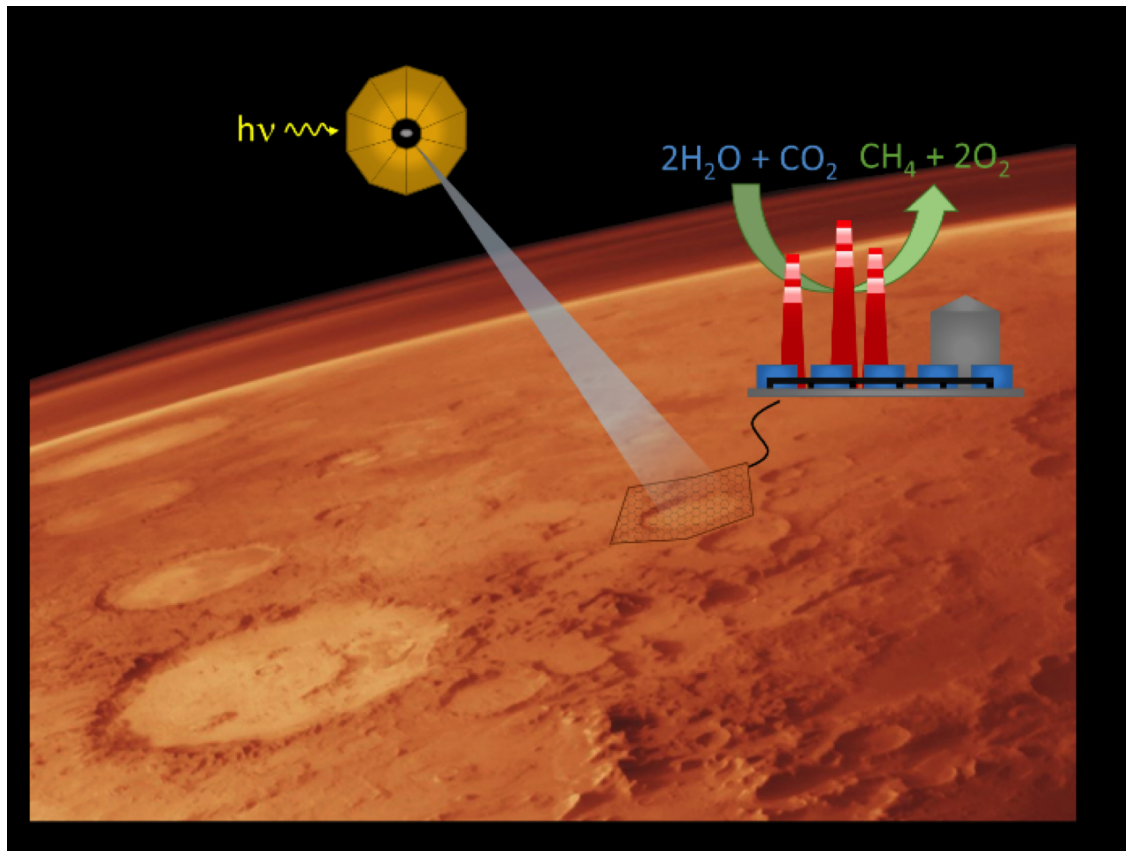
Figure 6.5: Concept of power beam-assisted CO_2 reduction.

this could have on the energy crisis that exists on Earth. The number of concerns regarding a similar system on Earth are significant but surmountable, and a technology demonstration on another planet could enable a more serious consideration of this type of power supply to solve our own energy challenges. Success of this technology would 1) enable a manned mission to the surface of Mars by supplying the power to produce fuel for ascent to allow the crew's return, 2) support a longer stay on the surface and provide infrastructure to eventually build a permanent base on the planet, 3) facilitate a higher science return by lessening Earth-based power delivery, and 4) possibly affect how we deal with the energy crisis here on Earth.

6.5   The Sabatier Reactor: Overview and Optimization Considerations

6.5.1   Sabatier Reactor Overview

In the case where purified water is available for ISRU conversion reactions, there are several means to take advantage of this key resource. As described above, the water can be used with atmospheric CO_2 in the aqueous PEC system to directly produce CH_4 and O_2. However, this

aqueous PEC TRL is quite low, and it may be more expedient to rely on higher TRL technologies to produce O_2 and CH_4. One such route is the electrolysis of water to H_2 and O_2 (a TRL 9 technology), followed by a Sabatier reaction of H_2 and CO_2.

The Sabatier reaction is a reversible, highly exothermic, and highly stable reaction for >95% methane production under selective catalyst and thermal conditions. Lower operating temperatures favor high conversion to CH_4 and H_2O, and the reaction is typically favorable at approximately $400^{\circ}C$. The Sabatier reaction is expressed in Equation 6.1.

$$CO_2 + 4\,H_2 \xrightarrow{\text{k + 1}} CH_4 + 2\,H_2O \qquad\qquad (6.1)$$

The methanation reaction via Sabatier has been investigated using various catalysts, including nickel (*Dew et al.*, 1955), Ruthenium on alumina (*Lunde & Kester*, 1973; *Muscatello et al.*, 2016; *Brooks et al.*, 2007), and Ruthenium on mixed phase TiO_2. A Sabatier assembly exists on the International Space Station (ISS) (*Samplatsky et al.*, 2011) for life-support systems, utilizing the CO_2 from waste cabin air. Sabatier systems are also being developed for deep space human missions to Mars as in-situ resource utilization (ISRU) applications (*Muscatello et al.*, 2016; *Junaedi et al.*, 2014; *Junaedi et al.*, 2011).

6.5.2 Sabatier Reactor Design Considerations

Different reactor designs have been proposed to increase the operating space velocities, long duration operation, and minimal mass. In particular, researchers have investigated microlith substrates (*Junaedi et al.*, 2014; *Junaedi et al.*, 2011), microchannel (*Brooks et al.*, 2007; *Thompson*, 2015), and packed bed reactors (*Muscatello et al.*, 2016; *Samplatsky et al.*, 2011) to optimize catalyst surface area, space velocity, high CO_2 conversion with high CH_4 selectivity, and thermodynamic controls. The mass, power, and operating ranges of these systems all vary widely in terms of the gas hourly space velocity (GHSV), temperature range, feed molar ratio, feed flow rate, and pressure, as displayed in Table 6.4.

The traditional packed bed Sabatier reactor is limited by the operational space velocities. The two reported microchannel reactors have varying GHSVs, while the microlith reactor has the highest performance for GHSV. Alternative reactor design can offer us ways of operating the Sabatier reactor at higher space velocities. The microlith (*Junaedi et al.*, 2014; *Junaedi et al.*, 2011) and microchannel (*Junaedi et al.*, 2011) style reactors offer higher GHSVs than the traditional packed bed reactor, while not compromising the conversion rates. Increasing the operating space velocities means that the reactor does not need to be as large, which can translate to mass reduction.

Stoichiometric feed conditions of the H_2:CO_2 ratio are due to applications. A life support application on ISS or in human presence with safety considerations runs CO_2 rich at sub Earth

Reactor	Type	Catalyst	Feed flow, SLPM	Feed H_2:CO_2	Pressure PSIA	Temperature °C	GHSV Hr^{-1}
ISS[a]	Packed Bed	Proprietary	3.2–9	3.5	<14.7	149–593 3 zones	N/A
KSC[b]	Packed Bed	Ru/Al$_2$O$_3$ pellets	3.75	4–4.5	40	180–500	2,500
PCI[c]	Microlith®	Ru or Rh coated microlith substrates	5.9–7.2	3.5–4.5	6–14.7	250–400	15,000– 20,000
Umpqua[d]	Microchannel	Ru on Al$_2$O$_3$	0.001–0.005	4	N/A	234–365 3 zones	2
PNNL[e]	Microchannel	Ru/TiO$_2$ on ceramic felt	0.1–0.25	4	14.7	250–400	7,200– 72,000

Table 6.4: Comparison of Sabatier reactor types and operational parameters

[a] *Samplatsky et al.* (2011)
[b] *Muscatello et al.* (2016)
[c] *Junaedi et al.* (2014); *Junaedi et al.* (2011)
[d] *Thompson* (2015)
[e] *Brooks et al.* (2007)

atmospheric pressures, and is typically turned on/off during use due to commodity availability. ISRU applications typically run H_2 rich at higher pressure with continuous operation.

It is important to design for material compatibility with water. Stainless steel can corrode or pit over time, and care must be considered for long-term use since the reaction has a primary product of water.

A particularly promising reactor is the Microlith®-based reactor developed by Precision Combustion, Inc. (PCI) (*Junaedi et al.*, 2011). The Microlith® substrate is made up on a series of "ultra-short-channel-length" metallic meshes that are wash coated with the desired catalyst. These Microlith® structures are reported to provide extremely good reaction rates that will allow us to operate the Microlith®-based Sabatier reactor at high space velocities. The rate of mass transfer-controlled reaction is directly related to the Geometric Surface Area (GSA) and inversely related to the boundary layer thickness. PCI's Microlith® has a higher GSA and a lower boundary layer thickness compared to a conventional Monolith and hence the mass transfer rates in a Microlith®-based reactor will be better than a monolith based reactor. The heat transfer properties of the Microlith® are also reported to be better than that of a conventional monolith. The superior heat transfer properties help with avoiding local hot spots and hence help to avoid catalyst sintering. It is to be noted that since a monolith-based reactor is already expected to be better than a packed bed reactor in terms of the heat and mass transfer properties, PCI's Microlith®-based reactor can be expected to perform significantly better that the traditional packed bed reactor. A successful mechanical vibration test was also performed on the reactor to

simulate launch vibration loads. The details of the test and its results can be found in *Junaedi et al.* (2011).

Finally, due to the lower channel length-to-diameter ratio (l/d) of the Microlith®, one would expect the pressure drop to be lower than that of a conventional monolith. However, since the Microlith®-based reactor has a more tortuous path for the reactants, it will also have a higher friction factor (f). Since the pressure drop is directly related both to f and l/d, the tradeoff between these two factors decides whether or not the Microlith®-based reactor will have a lower pressure drop than a conventional monolith. Presumably, there are some challenges with these Microlith® structures in terms of wash coating the catalyst and costs, as these structures are more sophisticated than conventional monoliths. However, at least in the near future, these challenges are more relevant for terrestrial applications than for space applications.

6.5.3   Sabatier Reactor System Design Considerations, Including Thermal Management

Managing heat from the exothermic process in Sabatier reactors is a complex task and to the best of our knowledge, it is not something that has not been demonstrated in the scale of interest for a human-rated ascent vehicle. The mass of the Sabatier system is comprised of the reactor mass and the mass of the ancillary equipment used for separation, storage, and heat management. Thus, in the search for an optimal solution to minimizing the mass of the Sabatier system, one possible design that is worth considering is catalyzed heat exchangers.

A catalyzed heat exchanger is made by depositing a catalyst on a heat transfer-friendly substrate. A design concept for catalyzed heat exchangers for steam reforming has been proposed by *Farrauto et al.* (2007). The idea was to couple steam reforming reactions (endothermic) to a combustion reaction (exothermic). They propose that this can be achieved by having two reaction chambers partitioned by a metal plate, with the steam reforming catalyst coated on one side and the combustion catalyst coated on the other. For our application, we can have a similar design with the Sabatier reaction (exothermic) on one side, coupled with a suitable endothermic reaction on the other.

A system design would include active thermal management from CO^2 and H^2 acquisition (cooler) and heat shedding required by the Sabatier reactor, to intertwine with the condenser for water extraction from the system. Two-phase materials, such as thermal wax, or active and passive cooling with reactor system inlet and outlet lines are one of the best ways to save mass and provide thermal management to a methanation system. The Curiosity Mars Rover also featured an advanced heat rejection system with hot and cold fluid loops for heating and cooling and thermal management. Integrating thermal management into the entire system can save mass and power.

Mass and power are not equally reported on the produced Sabatier reactor systems shown in Table 6.4. The KSC Sabatier reactor system is reported at 2 kg, while the PNNL microchannel system is reported at 0.09 kg and the PCI Microlith$^{\circledR}$ is reported at 1.75 kg. It is important to note that for a long-duration, deep space mission, a Sabatier reactor will be embedded into an entire autonomous system with controlled automation and active, unattended thermal management. The system hardware and thermal management will add to mass and a careful systems level approach will be performed to save on mass. The issue of cooling must be considered for Martian environments, as well as power cycles if a constant power source is not present. There will also be no opportunity to change out a spent or damaged catalyst bed if operating continuously without human interface for fuel production. This complexity adds to avionics, controls, redundancy, auto correction, and power systems that require a systems-level perspective for a mission with specific requirements. These system and fuel production requirements will dictate the approximate power and mass needed for a mission. For example, the work done on the Mars Atmospheric Conversion ISRU system at Kennedy Space Center considers the mass and power of the Sabatier reactor, cooling system, and Mars CO_2 acquisition hardware. Theoretical power estimates for a Mars Ascent Vehicle for a human Mars mission have been reported (*Muscatello et al.*, 2016), but Sabatier numbers have not yet been published.

6.5.4   Commodity Acquisition for the Sabatier Reactor

The design requirements for fuel production needed for a human-rated Mars Ascent Vehicle are currently not established. Estimates have been made of production rates and purity requirements. At Kennedy Space Center (KSC), the Mars Atmospheric ISRU system is sized for a Mars Sample Return mission, and currently ~$1/10^{th}$ the scale that would be needed for a human Mars mission ISRU fuel production depot (*Muscatello et al.*, 2016). Currently, the Mars Atmospheric Processing Module collects 88 g CO_2/hr from a simulated Mars atmosphere (95.4% CO_2, 3% nitrogen (N_2), and 1.6% argon (Ar)) and pressure. The system utilizes dual-operating cryocoolers for CO_2 acquisition from the Mars atmosphere, and is one consideration for collecting and separating the CO_2 from the Mars atmosphere. The current CO_2 collection rate produces 32 g/hr of CH_4 using the cryocoolers for CO_2 acquisition and the Sabatier reactor for CH_4 and H_2O production. In theory, the H_2 would be harvested from the H_2O extracted from excavated regolith that is collected from a soil hopper. This water or hydrated mineral would be separated from the regolith and cleaned in a water processing module, split with an electrolyzer or other available water-spitting technology, and H_2 would sustain the Sabatier reactor, while O_2 would be sent to liquefaction and storage.

From work at KSC on the cryocoolers and Sabatier Mars Atmospheric ISRU system, it was reported that for cryocooler operations in the laboratory with a Cryotel GT Cryocooler, the maximum cooling power froze 102 g CO_2/hr at approximately 158 W from a 240-W-capacity

cooler. This value can be scaled up to 680 W of total theoretical power needed for atmospheric acquisition to fuel a Mars ascent vehicle for a human mission.

6.6   Feedstock Collection

In any system designed to carry out ISRU conversion strategies, collecting, purifying, and handling of feedstock and product are important to consider. With regards to making oxygen and fuels on Mars, the two important feedstocks to deal with are CO_2 and H_2O.

CO_2 makes up the vast majority (~96%) of the thin atmosphere on Mars, with small amounts of Ar and N_2 (1.9% each) and traces of carbon monoxide, water, oxygen and methane. Dust storms on the surface of Mars represent another challenge in possible contaminants of feedstock. Depending on the chemical processes being used, these other components must be considered to determine if they will affect rates, yields, or lifetimes of the chemical conversion technology. Furthermore, because the Martian atmosphere is so thin (~6 mbar), concentration of the feedstock may be required. For the planned MOXIE instrument, the method of harvesting and concentrating CO_2 includes a filtered scroll compressor pump. Although the pump itself does not present any immediate concerns, dust mitigation presents a challenge due to a finite operation time of the filter from clogging by fine dust particles. Another previously considered method of harvesting CO_2 from the atmosphere involves the use of zeolites. This method is at a low TRL, with challenges involving pressure locking due to a buildup of the inert gases N_2 and Ar, and lack of methods for effectively sweeping them out of the vessel. Dust mitigation also poses a challenge for this method, as sealing a chamber is required. Methods such as filters, electrostatically enhanced cyclones, electrostatic precipitators, and Electrodynamic Dust Shields are all worth considering or expanding to address dust concerns, as Martian dust is expected to be a difficulty for many planned processes.

Water harvesting represents a very different type of challenge—the water in the Mars atmosphere is present in only trace amounts, so in order to collect enough water for the proposed chemical processes (or for other future human needs), the method used must collect and purify water from the regolith. Even though the requirements for ISRU fuel production and, for example, drinking water may differ, it is worth considering what differing technologies offer because it is unlikely that more than one method will be used. It is of course possible that one method will not fulfill all requirements and that further purification will be required for some water uses and not others, however all purposes should be considered when choosing a water harvesting technology. The water on Mars exists in the form of hydrated minerals or ice. A water collection method must be extremely efficient given the number of processes that will eventually require water and handling methods must likewise protect against losses to the environment. Furthermore, purity is also particularly important, as contamination may destroy catalysts, to say nothing of purity requirements for manned missions. No existing technology has been identified to fulfill this

requirement. A technology demonstration (HABIT) on board the ExoMars lander including water harvesting was planned, where exposed salts would absorb atmospheric water and presumably be vacuum transferred for collection. While the mission expected to see approximately 50 L/year of water collection, this method alone is unlikely to meet requirements such as those posed for manned missions due to the extremely low levels of atmospheric water. However, it is worth noting this as a possible collection and purification pathway, should a process to liberate gaseous water from the regolith be developed. A low TRL method for water harvesting has been proposed to do this using microwaves directed at hydrated minerals. This has been demonstrated on small samples with approximately 60% efficiency, but in the current batch-mode design, it is impractical for the large amounts of water needed for a manned Mars mission. Currently, there does not yet exist a method to harvest water in the volumes that will be necessary to support ISRU strategies on the surface of Mars.

Each method that was considered in this workshop involved the deployment of a large surface structure. Because of this, methods taking advantage of the large surface area were considered to address the water harvesting challenge. These techniques involve the use of a lightweight, deployable, large-surface-area bagging operation to facilitate localized removal of water from the Martian surface underneath, humidifying the atmosphere inside the structure. Native Martian heating could be used passively, or alternatively directed microwaves generated from the backside of the structure might be used to improve efficiency. Once the water has been removed from the Martian soil, a highly efficient collection method is required to pull the water back out of the structure's interior before it is lost to the Martian atmosphere. Coupling technologies such as the salts in the aforementioned HABIT collection concept with directional air flow may be sufficient to harvest the water, followed by vacuum transfer to generate a purified water sample ready for use. Based on an assumed microwave penetration depth of ~1m, 80% microwave absorption, and 6 wt% H_2O present in Martian regolith, a calculated 2.8 t of water can be harvested from a 70×70 m microwave beam spot over 500 sols.

6.7   Roll-Up of System Engineering Considerations

A preliminary mass calculation was carried out for a notional PEC array assembly. The following bill of materials was created for each layer in the assembly (see Table 6.5)

With this bill of materials, the area-specific density of a PEC array is projected to be ~0.33 kg/m^2. A 20% margin was added on to account for additional structural support and to account for the low maturity of the PEC array design, which results in an area-specific density of 0.4 kg/m^2. For a baseline 10% of a full-sized system of 121 m^2, this results in a mass estimate of approximately 50 kg for the PEC array alone. To determine the mass of the gas manifold, carbon fiber-reinforced polymer manifold designs for terrestrial applications were scaled to this application. This resulted in a mass estimate of 13.4 kg for manifolds for a 121-m^2 array.

Material	Area Density (g/m^2)	Purpose
Containment Layer		
Cover Glass (70 µm)	166	To provide structural integrity to the system This thickness was derived from a preliminary stress analysis using equations for an elliptical pressure vessel with a safety factor of 2. Density value from specification sheet at www.corning.com
Photovoltaic Layer		
PV Materials and Contacts	20	Provide light absorption to drive the reaction
Kapton film (15 µm)	2	Provide support.[a]
MEA Layer		
Oxidation Catalysts	N/A	Increase kinetic of the reaction. Note that mass contribution is assumed to be very low.
Carbon Fiber (25 µm)	25	Catalyst support
Nafion (50 µm)	50	Ionic transport and prevention of reactant gas crossover
Reduction Catalysts	N/A	Increase kinetic of the reaction. Note that mass contribution is assumed to be very low.

Table 6.5: Materials for a notional PEC array assembly.

[a]http://www.dupont.com/content/dam/dupont/products-and-services/membranes-and-films/polyimde-films/documents/DEC-Kapton-summary-of-properties.pdf

7. Recommendations for Future Work

The following are brief recommendations for future work to mature the PEC and EC technologies, as well as to provide better estimates of performance metrics to facilitate higher fidelity trade studies:

1. Develop prototype $25°C$ operation $CO_2 \longrightarrow CO + O_2$ devices with existing materials ("Device-A") to at least TRL 4 to enable meaningful system-level comparisons with SOXE devices.

2. Establish CH_4-generating catalytic systems capable of operating at $25°C$ using CO_2 and H_2 or H_2O as inputs.

3. Develop prototype $25°C$ operation CH_4-generating devices ("Device-B") to at least TRL 4 and compare system-level metrics to the H_2O electrolysis/Sabatier approach.

4. Establish a materials set for a non-aqueous CO_2 reduction PEC device ("Device-C") and characterize at TRL 4.

5. Evaluate the integration of TRL 4 devices above with PV arrays vs. direct PEC operation.

6. Assess the feasibility of power beaming approaches to supply PV power to landed energy storage arrays.

References

Arya, M., Lee, N., & Pellegrino, S. (2016). Ultralight structures for space solar power satellites. In *3rd AIAA Spacecraft Structures Conference* (p. 1950).

Arya, M., Lee, N., & Pellegrino, S. (2017). Crease-free biaxial packaging of thick membranes with slipping folds. *International Journal of Solids and Structures*, 108, 24-39.

Asadi, M., Kim, K., Liu, C., Addepalli, A. V., Abbasi, P., Yasaei, P., ... & Zapol, P. (2016). Nanostructured transition metal dichalcogenide electrocatalysts for CO2 reduction in ionic liquid. *Science*, 353(6298), 467-470.

Batchellor, A. S., & Boettcher, S. W. (2015). Pulse-electrodeposited Ni–Fe (oxy) hydroxide oxygen evolution electrocatalysts with high geometric and intrinsic activities at large mass loadings. *ACS Catalysis*, 5(11), 6680-6689.

Berger, A., Segalman, R. A., & Newman, J. (2014). Material requirements for membrane separators in a water-splitting photoelectrochemical cell. *Energy & Environmental Science*, 7(4), 1468-1476.

Breedlove, B. K., Ferrence, G. M., Washington, J., & Kubiak, C. P. (2001). A photoelectrochemical approach to splitting carbon dioxide for a manned mission to Mars. *Materials & Design*, 22(7), 577-584.

Brooks, K. P., Hu, J., Zhu, H., & Kee, R. J. (2007). Methanation of carbon dioxide by hydrogen reduction using the Sabatier process in microchannel reactors. *Chemical Engineering Science*, 62(4), 1161-1170.

Chen, Y., Li, C. W., & Kanan, M. W. (2012). Aqueous CO_2 reduction at very low overpotential on oxide-derived Au nanoparticles. *Journal of the American Chemical Society*, 134(49), 19969-19972.

Crow, S., & Crow, S. (1997). The MOXCE Project-New cells for producing oxygen on Mars. In *33rd Joint Propulsion Conference and Exhibit* (p. 2766).

Dew, J. N., White, R. R., & Sliepcevich, C. M. (1955). Hydrogenation of carbon dioxide on nickel-kieselguhr catalyst. *Industrial & Engineering Chemistry*, 47(1), 140-146.

Drake, B.G. (2009), Human Exploration of Mars Design Reference Architecture (DRA) 5.0, NASA Special Report, NASA SP-2009-566.

Drake, B. G., Hoffman, S. J., & Beaty, D. W. (2010, March). Human exploration of Mars, design reference architecture 5.0. In *Aerospace Conference, 2010 IEEE* (pp. 1-24). IEEE.

Farrauto, R. J., Liu, Y., Ruettinger, W., Ilinich, O., Shore, L., & Giroux, T. (2007). Precious metal catalysts supported on ceramic and metal monolithic structures for the hydrogen economy. *Catalysis Reviews*, 49(2), 141-196.

Fogg, P. G. (Ed.). (2017). *Carbon Dioxide in non-aqueous solvents at pressures less than 200 kPa* (Vol. 50). Elsevier.

Freeman, B., Yampolskii, Y., & Pinnau, I. (Eds.). (2006). *Materials science of membranes for gas and vapor separation*. John Wiley & Sons.

R.H. Frisbee, J.R. French, Jr. and E.A. Lawton. (1987). A new look at oxygen production on Mars-In situ propellant production (ISPP). In *25th AIAA Aerospace Sciences Meeting* (p. 236).

Froehlich, J. D., & Kubiak, C. P. (2015). The homogeneous reduction of CO_2 by [Ni (cyclam)]$^+$: increased catalytic rates with the addition of a CO scavenger. *Journal of the American Chemical Society*, 137(10), 3565-3573.

Gendron, S., Wang, G., Jiang, X. X., Nikanpour, D., Davis, J., Lange, C., & Lapensée, S. (2010). Phoenix mars lander mission: Thermal and cfd modeling of the meteorological instrument based on flight data. In *40th International Conference on Environmental Systems* (p. 6195).

Gennaro, A., Isse, A. A., Severin, M. G., Vianello, E., Bhugun, I., & Savé ant, J. M. (1996). Mechanism of the electrochemical reduction of carbon dioxide at inert electrodes in media of low proton availability. *Journal of the Chemical Society, Faraday Transactions*, 92(20), 3963-3968.

Gerischer, H. (1979). Solar photoelectrolysis with semiconductor electrodes. In *Solar energy conversion* (pp. 115-172). Springer, Berlin, Heidelberg.

Gibson, M. A., Oleson, S. R., Poston, D. I., & McClure, P. (2017). NASA's Kilopower Reactor Development and the Path to Higher Power Missions.

Haber, J. A., Cai, Y., Jung, S., Xiang, C., Mitrovic, S., Jin, J., ... & Gregoire, J. M. (2014). Discovering Ce-rich oxygen evolution catalysts, from high throughput screening to water electrolysis. *Energy & Environmental Science*, 7(2), 682-688.

Hartvigsen, J. J., Elangovan, S., Larsen, D., Elwell, J., Bokil, M., Frost, L. J., & Clark, L. M. (2015). Challenges of Solid Oxide Electrolysis for Production of Fuel and Oxygen from Mars Atmospheric CO_2. *ECS Transactions*, 68(1), 3563-3583.

Hawecker, J., Lehn, J. M., & Ziessel, R. (1984). Electrocatalytic reduction of carbon dioxide mediated by $Re(bipy)(CO)_3Cl$ (bipy= 2, 2'-bipyridine). *Journal of the Chemical Society, Chemical Communications*, (6), 328-330.

Hecht, M. (2016). MOXIE Mars Oxygen ISRU Experiment, KISS Workshop *Addressing the Mars ISRU Challenge: Production of Oxygen and Fuel from CO_2 using Sunlight*, California Institute of Technology (June 28-July 1, 2016).

Hoffman, J. A., Rapp, D., & Hecht, M. (2015). The Mars Oxygen ISRU Experiment (MOXIE) on the Mars 2020 Rover. In *AIAA SPACE 2015 Conference and Exposition* (p. 4561).

Hori, Y., Murata, A., & Takahashi, R. (1989). Formation of hydrocarbons in the electrochemical reduction of carbon dioxide at a copper electrode in aqueous solution. *Journal of the Chemical Society, Faraday Transactions 1: Physical Chemistry in Condensed Phases*, 85(8), 2309-2326.

Hori, Y. I. (2008). Electrochemical CO_2 reduction on metal electrodes. In *Modern aspects of electrochemistry* (pp. 89-189). Springer, New York, NY.

Horn, N. R., & Paul, D. R. (2011). Carbon dioxide plasticization and conditioning effects in thick vs. thin glassy polymer films. *Polymer*, 52(7), 1619-1627.

Huang, Y., & Paul, D. R. (2004). Physical aging of thin glassy polymer films monitored by gas permeability. *Polymer*, 45(25), 8377-8393.

Infelta, P. P., De Haas, M. P., & Warman, J. M. (1977). The study of the transient conductivity of pulse irradiated dielectric liquids on a nanosecond timescale using microwaves. *Radiation Physics and Chemistry* (1977), 10(5-6), 353-365.

Jorapur, Y. R., & Chi, D. Y. (2005). Synthesis of symmetrical organic carbonates via significantly enhanced alkylation of metal carbonates with alkyl halides/sulfonates in ionic liquid. *Journal of organic chemistry*, 70(26), 10774-10777.

Junaedi, C., Hawley, K., Walsh, D., Roychoudhury, S., Abney, M., & Perry, J. (2011, July). Compact and lightweight sabatier reactor for carbon dioxide reduction. In *41st International Conference on Environmental Systems* (p. 5033).

Junaedi, C., Hawley, K., Walsh, D., Roychoudhury, S., Abney, M. B., & Perry, J. L. (2014). CO_2 reduction assembly prototype using microlith-based sabatier reactor for ground demonstration. In *44th International Conference on Environmental Systems*.

Jung, S., McCrory, C. C., Ferrer, I. M., Peters, J. C., & Jaramillo, T. F. (2016). Benchmarking nanoparticulate metal oxide electrocatalysts for the alkaline water oxidation reaction. *Journal of Materials Chemistry A*, 4(8), 3068-3076.

Kuhl, K. P., Cave, E. R., Abram, D. N., & Jaramillo, T. F. (2012). New insights into the electrochemical reduction of carbon dioxide on metallic copper surfaces. *Energy & Environmental Science*, 5(5), 7050-7059.

Lei, Z., Dai, C., & Chen, B. (2013). Gas solubility in ionic liquids. *Chemical reviews*, 114(2), 1289-1326.

Lewis, J. S. (1993). *Resources of near-earth space*. The University of Arizona Press (p 799).

Lu, Q., Rosen, J., Zhou, Y., Hutchings, G. S., Kimmel, Y. C., Chen, J. G., & Jiao, F. (2014). A selective and efficient electrocatalyst for carbon dioxide reduction. *Nature communications*, 5, 3242.

Lunde, P. J., & Kester, F. L. (1973). Rates of methane formation from carbon dioxide and hydrogen over a ruthenium catalyst. *Journal of Catalysis*, 30(3), 423-429.

McCrory, C. C., Jung, S., Ferrer, I. M., Chatman, S. M., Peters, J. C., & Jaramillo, T. F. (2015). Benchmarking hydrogen evolving reaction and oxygen evolving reaction electrocatalysts for solar water splitting devices. *Journal of the American Chemical Society*, 137(13), 4347-4357.

Merle, G., Wessling, M., & Nijmeijer, K. (2011). Anion exchange membranes for alkaline fuel cells: A review. *Journal of Membrane Science*, 377(1-2), 1-35.

Meyen, F. E., Hecht, M. H., Hoffman, J. A., & MOXIE Team. (2016). Thermodynamic model of Mars Oxygen ISRU Experiment (MOXIE). *Acta Astronautica*, 129, 82-87.

Mikulas, M. M., Collins, T. J., Doggett, W., Dorsey, J., & Watson, J. (2006, January). Truss performance and packaging metrics. In *AIP Conference Proceedings* (Vol. 813, No. 1, pp. 1000-1009). AIP.

Miura, K. (1985). Method of packaging and deployment of large membranes in space. *Institute of Space and Astronautical Science report*, 618, 1.

Murphy, T. M., Langhe, D. S., Ponting, M., Baer, E., Freeman, B. D., & Paul, D. R. (2011). Physical aging of layered glassy polymer films via gas permeability tracking. *Polymer*, 52(26), 6117-6125.

Muscatello, A., Hintze, P., Meier, A., Bayliss, J., Karr, L., Paley, S., ... & Lunn, G. (2016). Mars Atmospheric In Situ Resource Utilization Projects at the Kennedy Space Center. *Earth and Space*, 449.

Papa, A., & Pellegrino, S. (2008). Systematically creased thin-film membrane structures. *Journal of Spacecraft and Rockets*, 45(1), 10-18.

Rapp, D. (2016). *Human Missions to Mars*. 2nd Ed., Springer.

Ratliff, K. S., Lentz, R. E., & Kubiak, C. P. (1992). Carbon dioxide chemistry of the trinuclear complex $[Ni_3(\mu_3\text{-}CNMe)(\mu_3\text{-}I)(dppm)_3][PF_6]$. Electrocatalytic reduction of carbon dioxide. *Organometallics*, 11(6), 1986-1988.

Richter, R. (1981). Basic investigation into the production of oxygen in a solid electrolyte process. In *16th Thermophysics Conference* (p. 1175).

Rucker, M. A., Oleson, S. R., George, P., Landis, G., Fincannon, J., Bogner, A., ... & Gyekenyesi, J. (2016). Solar vs. Fission Surface Power for Mars. In *AIAA SPACE 2016* (p. 5452).

Samplatsky, D., Grohs, K., Edeen, M., Crusan, J., & Burkey, R. (2011). Development and Integration of the Flight Sabatier Assembly on the ISS. In *41st International Conference on Environmental Systems* (p. 5151).

Sampson, M. D., & Kubiak, C. P. (2016). Manganese electrocatalysts with bulky bipyridine ligands: utilizing Lewis acids to promote carbon dioxide reduction at low overpotentials. *Journal of the American Chemical Society*, 138(4), 1386-1393.

Sanders, G. B., Paz, A., Oryshchyn, L., Araghi, K., Muscatello, A., Linne, D. L., ... & Peters, T. (2015). Mars ISRU for Production of Mission Critical Consumables-Options, Recent Studies, and Current State of the Art. In *AIAA SPACE 2015 Conference and Exposition* (p. 4458).

Seo, S., DeSilva, M. A., & Brennecke, J. F. (2014). Physical properties and CO2 reaction pathway of 1-ethyl-3-methylimidazolium ionic liquids with aprotic heterocyclic anions. *Journal of Physical Chemistry B*, 118(51), 14870-14879.

Sridhar, K. R., & Vaniman, B. T. (1997). Oxygen production on Mars using solid oxide electrolysis. *Solid State Ionics*, 93(3-4), 321-328.

Sun, K., Saadi, F. H., Lichterman, M. F., Hale, W. G., Wang, H. P., Zhou, X., ... & Brunschwig, B. S. (2015). Stable solar-driven oxidation of water by semiconducting photoanodes protected

by transparent catalytic nickel oxide films. *Proceedings of the National Academy of Sciences*, 112(12), 3612-3617.

Thompson, J. O. (2015, July). Scaleable, High Efficiency Microchannel Sabatier Reactor. *45th International Conference on Environmental Systems.*

Twigg, M. V. (2007). Progress and future challenges in controlling automotive exhaust gas emissions. *Applied Catalysis B: Environmental*, 70(1-4), 2-15.

Umland, J., & Eisen, H. (2001, April). SRTM on-orbit structural dynamics. In *19th AIAA Applied Aerodynamics Conference* (p. 1588).

Varcoe, J. R., Atanassov, P., Dekel, D. R., Herring, A. M., Hickner, M. A., Kohl, P. A., ... & Xu, T. (2014). Anion-exchange membranes in electrochemical energy systems. *Energy & environmental science*, 7(10), 3135-3191.

Vega, J. A., Chartier, C., & Mustain, W. E. (2010). Effect of hydroxide and carbonate alkaline media on anion exchange membranes. *Journal of Power Sources*, 195(21), 7176-7180.

Wang, S., Li, X., Wu, H., Tian, Z., Xin, Q., He, G., ... & Guiver, M. D. (2016). Advances in high permeability polymer-based membrane materials for CO_2 separations. *Energy & Environmental Science*, 9(6), 1863-1890.

White, S., Spence, B., Trautt, T., & Cronin, P. (2007, June). UltraFlex-175 on Space Technology 8 (ST8)—Validating the Next-Generation in Lightweight Solar Arrays. *Proceedings of NASA Science and Technology Conference*, University of Maryland (Jun. 19-21, 2007).

Winslow, C. (1993). Space station freedom solar array design development. *IEEE Aerospace and Electronic Systems Magazine*, 8(1), 3-8.

Zhang, S., Lu, X., Zhou, Q., Li, X., Zhang, X., & Li, S. (2009). *Ionic liquids: physicochemical properties.* Elsevier.

Zhang, X., Li, X., Zhang, D., Su, N. Q., Yang, W., Everitt, H. O., & Liu, J. (2017). Product selectivity in plasmonic photocatalysis for carbon dioxide hydrogenation. *Nature communications*, 8, 14542.